UNIVERSITEIT • STELLENBOSCH • UNIVERSITY

The Feedback Control Of A Robotic Gymnast

by

Henry Kotzé

Mechatronic Project 448

Report submitted in partial fulfilment of the requirements of the module Mechatronic Project 448 for the degree Baccalaureus in Engineering in the Department of Mechanical and Mechatronic Engineering at the University of Stellenbosch

Study leader: Dr. J.A.A Engelbrecht

October 11, 2018

Declaration

By submitting this thesis electronically, I declare that the entirety of the work contained therein is my own, original work, that I am the sole author thereof (save to the extent explicitly otherwise stated), that reproduction and publication thereof by Stellenbosch University will not infringe any third party rights and that I have not previously in its entirety or in part submitted it for obtaining any qualification.

Date: 2018/10/27 .....

Abstract

The Feedback Control of a Robotic Gymnast

H. Kotzé

Department of Mechanical and Mechatronic Engineering,
University of Stellenbosch,
Private Bag X1, Matieland 7602, South Africa.

Thesis: BEng (Mechatronics)

October 2018

meep

Uittreksel

Die Terugvoer Beheer van 'n Robotiese Gimnas

("The Feedback Control of a Robotic Gymnast")

H. Kotzé

Departement Meganiese en Megatroniese Ingenieurswese,
Universiteit van Stellenbosch,
Privaatsak X1, Matieland 7602, Suid Afrika.

Tesis: BIng (Megatronika)

Oktober 2018

meep

Acknowledgements

I would like to express my sincere gratitude to the following people and organisations.

Dedications

Hierdie tesis word opgedra aan ...

Contents

List of Figures

List of Tables

Nomenclature

Constants

g =	$9.81\,\mathrm{m/s^2}$	

Variables

Re_D	Reynolds number (diameter)	[ ]
x	Coordinate	[m]
$\ddot{x}$	Acceleration	[$\mathrm{m/s^2}$]
θ	Rotation angle	[rad]
τ	Moment	[N·m]

Vectors and Tensors

$\overrightarrow{v}$	Physical vector, see equation ...

Subscripts

a	Adiabatic
a	Coordinate

Chapter 1

Introduction

1.1 Problem Statement

A feedback control system for a robotic gymnast that is able to swing from the "hanging" position to the "handstand" position must be designed, implemented and verified. Feedback control loops must be designed that use the "legs" of the gymnast to swing the "body" of the gymnast from the "hanging" position to a "handstand" position and then balance the gymnast on top of the horizontal bar. A mathematical model for the dynamics of the swinging robotic gymnast system must be derived or sourced from literature. The dynamics are analysed to propose an appropriate feedback control architecture that actuates the "legs" of the gymnast using feedback from sensors that measure the swinging motion of the gymnast on a horizontal bar. A practical demonstrator must be constructed and the correct operation must be demonstrated.

1.2 Literature Study

There are a few design approaches to the swing-up and balancing of the robotic gymnast. This problem is also known as the swinging acrobat.

1.3 System Overview

Figure 1.1 provides an overview of the various subsystems the project will contain. The project is subdivided into these subsystems being developed separately with little interaction between the each other. An brief overview on each subsystem will be presented here.

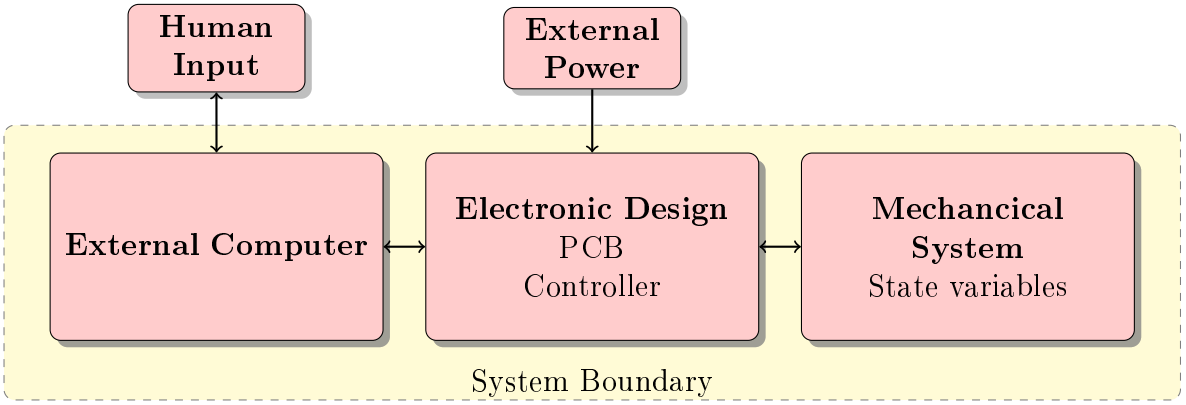

Figure 1.1: System Overview of the Feedback Control of Robotic Gymnast

The external computer communicates with the electronic design sending instruction to start the system and for debugging purposes. The external computer will receive data from the electronic design and allows the verification of system parameters.

The electronic design acts as the middle-man between the mechanical design and the external computer. It provides instructions to the mechanical design components based on the controller while sending data to the external computer. The electronic design contains the Printed Circuit Board (PCB) that conditions all the signals for processing.

The mechanical design was responsible for creating a physical model that represents the mathematical model describing the system. The correct sensors must be selected to measure the state variables and providing interfaces for the electronic design.

1.4 Project Execution

The execution of the project occurs in a sequence of steps. First the mathematical model of the system is derived by using the appropriate approaches. The derived mathematical model is then implemented on a simulation program where the dynamics of the system can be verified and inspected.

Following the successful implementation of the mathematical model the various controllers will be designed and implemented on the simulation program. The behaviour of the simulated system will be inspected.

From the simulation results the mechanical design specification will be determined. The mechanical design will then commence to create a physical model that provides an acceptable representation of the mathematical model.

During manufacturing of the mechanical design the electronic design will start. Conceptual designs will be done to determine the various designs capable of meeting the requirements. The electronic design will be tested to ensure it performs as designed with the opportunity to create revisions of the design.

The programming of the micro-controller will start. This includes the programming of the controller, data acquisition and the conversions of the sampled data.

System identification will then occur to determine the various parameters required by the controllers. These newly determined parameters will then be implemented on the simulation program. Existing controllers will be updated and verified in simulation.

The updated controllers are then implemented onto the microcontroller for the system experiments to start. From these system experiments the responses of the experiment will be compared by those of the simulation.

The report was written throughout the sequence of steps mentioned above and will be completed and reviewed at the end.

1.5 Report Outline

A brief overview of each chapter in the report will provided here. It acts as primer for the reader and the easy identification of section that may interest the reader more.

Chapter 2 explain the system concepts that is reference throughout the report. It contains the mathematical derivation of the robotic gymnast and the simulated model. The system parameters with system identification test are shown and whether the simulated models is a acceptable representation of the physical model.

Chapter 3 describes the design paradigm to swinging and balancing of the robotic gymnast. The specification for the controllers and the simulated responses of the controller are provided.

Chapter 4 contains the designs of the mechanical and electronic system of the project. The various components used in the designs and it explains how

the physical model state information is provided to the designed controllers.

Chapter 5 describe the software implemented to reduplicate what has been done in the project. It explains the architecture of the software and the various functions implemented.

Chapter 6 provides the practical results of the controllers implemented in chapter 3 and hypothise unexpected behaviour in the experiments.

Chapter 7 concludes the report with a summary of the report and recommendation for future endeavours on the Feedback Control of a Robotic Gymnast.

Chapter 2

Conceptualisation and Modelling

2.1 System Concepts

The report contains many variable names and use of terminology for concepts that is used throughout the report. These variables and terminologies are defined here.

The double pendulum is a under-actuated system which is defined as a system where the input to the system cannot command any of the state variables an instantaneous acceleration (Tedrake). This is due to the torque input only actuating the lower pendulum and the energy in the lower pendulum must be transferred to the upper pendulum to initiate an acceleration.

The robotic gymnast is describe as a double pendulum consisting out of an actuated- and non-actuated pendulum as seen in Figure 2.1. The position of the non-actuated pendulum is described by the angle θ whereas the actuated pendulum is described by ϕ relative to θ. The angle's θ and ϕ are the independent parameters that describe the entire system.

There are 2 position of interest where the system contain special characteristics. These 2 positions are the stable- and unstable equilibrium position. In the stable position the system is at rest hanging downwards where both θ and $\phi = 0\,\text{rad}$. It is stable due to the system containing negative real poles resulting in the system returning to this position when disturbed. The unstable equilibrium position is where $\theta = 2\pi\,\text{rad}$ and $\phi = 0\,\text{rad}$ resulting in the robotic gymnast balancing in the inverted position. In this position the system contains positive real poles and any disturbance will cause the system to grow away from this position.

region of controllability:he null controllability region is the set of states that can be steered to inverted unstable equilibrium position in a fixed time

with a constrained control input nul (2002).

LTI system

2.2 Mathematical Model

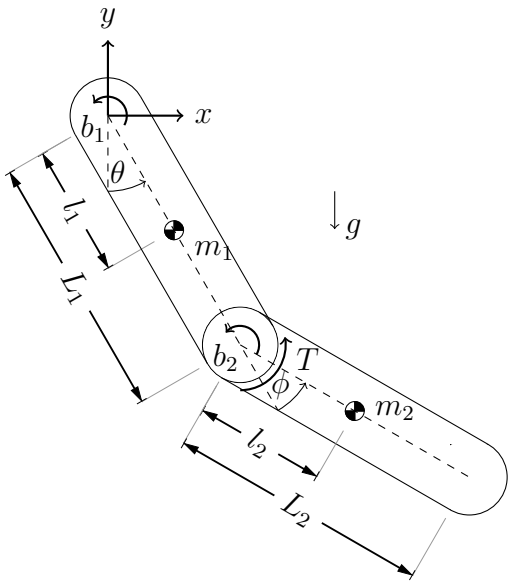

Figure 2.1: Free Body Diagram of the Double Pendulum

The approach taken to derive the mathematical model of the robotic gymnast will be presented in this section. It is presented to allow the reader to understand parameters used throughout the report and critical to the implementation of the swing-up controller. The swinging of the robotic gymnast consist of non-linear behaviour and it is require to fully derive the dynamics of the system. The strenuous mathematical steps are removed from the reader and provided in Appendix A.1. A summary of the motivation and paradigm approach to the derivation is provided here.

Figure 2.1 shows the free body diagram of the robotic gymnast which was modelled as two pendulums connected together with a hinge. Each pendulum was modelled as having their mass distributed arbitrary along their axis. A torque is actuating the lower pendulum and friction was modelled as a function of the angular velocity.

The Euler-Lagrange equation shown in (2.1) was used to derive the dynamics of the system by analysing the energy of the system which is easily defined as the potential energy T and the kinetic energy V of the 2 pendulums.

$$\frac{d}{dt}\frac{\partial \mathcal{L}}{\partial \vec{\dot{q}}} - \frac{\partial \mathcal{L}}{\partial \vec{q}} = 0 \tag{2.1}$$

$$\mathcal{L} = T - V \tag{2.2}$$

Using the Euler-Lagrange equation leads to the condense equations shown in (2.3) and (2.4),

$$d_{11}\ddot{\theta} + d_{12}\ddot{\phi} + h_1 + \psi_1 = 0 \tag{2.3}$$

$$d_{21}\ddot{\theta} + d_{22}\ddot{\phi} + h_2 + \psi_2 = \tau \tag{2.4}$$

where the coefficients are defined as

$$d_{11} = I_a + I_b + m_2(L_1^2 + l_2^2 + 2L_1 l_2 \cos(\phi)) \tag{2.5}$$

$$d_{12} = I_b + m_2(l_2^2 L_1 l_2 \cos(\phi)) \tag{2.6}$$

$$h_1 = -m_2 L_1 l_2 \sin(\phi)\dot{\phi}^2 - 2m_2 L_1 l_2 \sin(\phi)\dot{\phi}\dot{\theta} \tag{2.7}$$

$$\psi_1 = (m_2 l_1 + m_2 L_1) g \cos(\theta) + m_2 l_2 g \cos(\theta + \phi) + f_{c_1} \tag{2.8}$$

$$d_{21} = I_b + m_2(l_2^2 + L_1 l_2 \cos(\phi)) \tag{2.9}$$

$$d_{22} = I_b + m_2 l_2^2 \tag{2.10}$$

$$h_2 = m_2 L_1 l_2 \sin(\phi)\dot{\theta}^2 \tag{2.11}$$

$$\psi_2 = m_2 l_2 g \cos(\theta + \phi) + f_{c_2} \tag{2.12}$$

The friction that develops in the pendulums are for now represented by the f_{c_1} and f_{c_2} terms and will be expanded in the system identification section.

2.3 Simulation Model

The mathematical model derived in the previous section was required to be implemented on a simulation program. Simulating the model allows the designer to understand how system parameters influence the dynamics of the system and the verification of controllers implemented. It will be presented by discussing the non-linearities added to represent the physical model beter.

Simulation of the robotic gymnast was done using MATLAB Simulink. The differential equations shown in equation (2.3) and (2.4) were implemented using the *MATLAB Function* box. It was required to write $\ddot{\phi}$ and $\ddot{\theta}$ as the subject in each of the *MATLAB Function* box to allow MATLAB to simulate the model.

Non-linear behaviour introduced by sensors and components were added such as saturation of the motor torque, gearbox backlash and quantisation of sensory data. These non-linearities were implemented to allow the simulation to be an acceptable representation of the physical system. The Simulink Model used for simulation is shown in Figure 2.2.

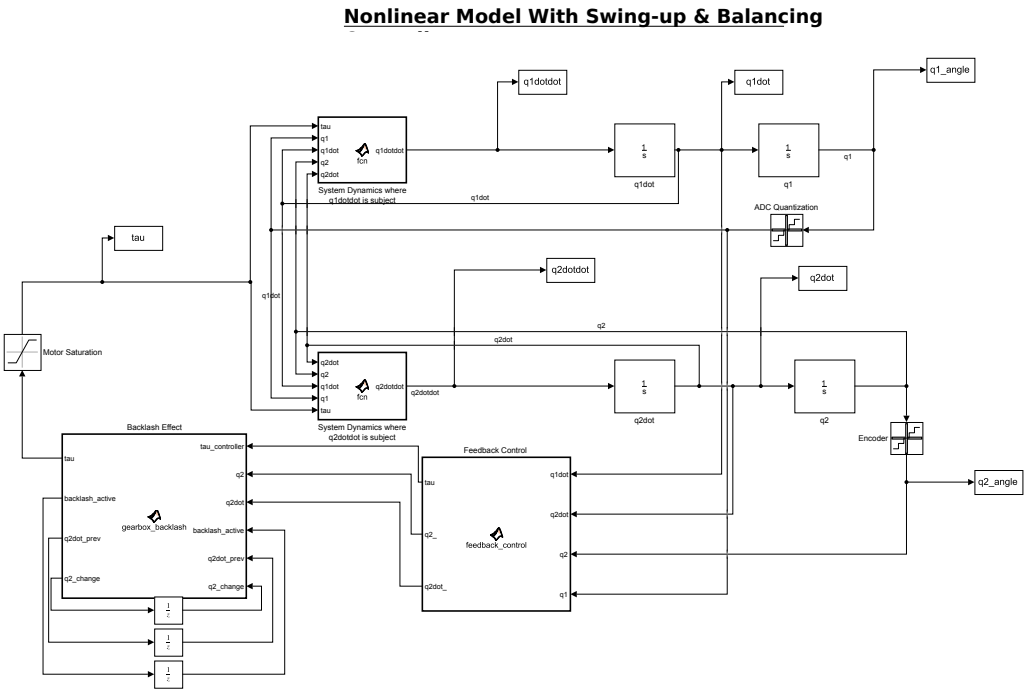

Figure 2.2: MATLAB Simulink Model

2.4 System Identification

The system identification tests are done to determine the characteristics that describe the behaviour of the system. These characteristics include the damping ratio's and natural frequencies of the system. These characteristics will be presented by showing measured responses and how these responses can be modelled.

The project started off with a previous physical model which provided realistic system parameters to allow the simulation to be an acceptable representation of a physical model. From using these previous system parameters the simulation provided a set of specification for the new mechanical design. All responses shown and values calculated are based of the new mechanical design parameters shown in Table 2.1.

The system is described by 2 independent parameters and is expected to contain 2 natural frequencies each accompanied by a damping coefficient. The first natural frequency of the system was determined by inspecting the response of the system when starting at a initial condition and keeping $\phi = 0\,\text{rad}$ throughout the response. This was done by using a lightweight PVC pipe that has negligible effect on the weight of the system. The actuated pendulum and non-actuated pendulum are constrained to this pipe to ensure the 2 pendulums stay in-line with each other and thus ensuring $\phi = 0\,\text{rad}$. The response of the

System Parameter	Value
L_1	$0.235\,\mathrm{m}$
L_2	$0.314\,\mathrm{m}$
I_A	$0.0022\,\mathrm{kg}\cdot\mathrm{m}^2$
I_B	$0.0054\,\mathrm{kg}\cdot\mathrm{m}^2$
m_1	$0.576\,\mathrm{kg}$
m_2	$0.492\,\mathrm{kg}$
l_1	$0.205\,\mathrm{m}$
l_2	$0.238\,\mathrm{m}$

Table 2.1: System Parameters

system is shown in Figure 2.3 starting at a initial condition of roughly $\theta = \frac{\pi}{6}$. The accuracy of the initial conditions is of little importance, but the initial condition must allow the response to contain a few oscillation to accurately determine the parameter of interest.

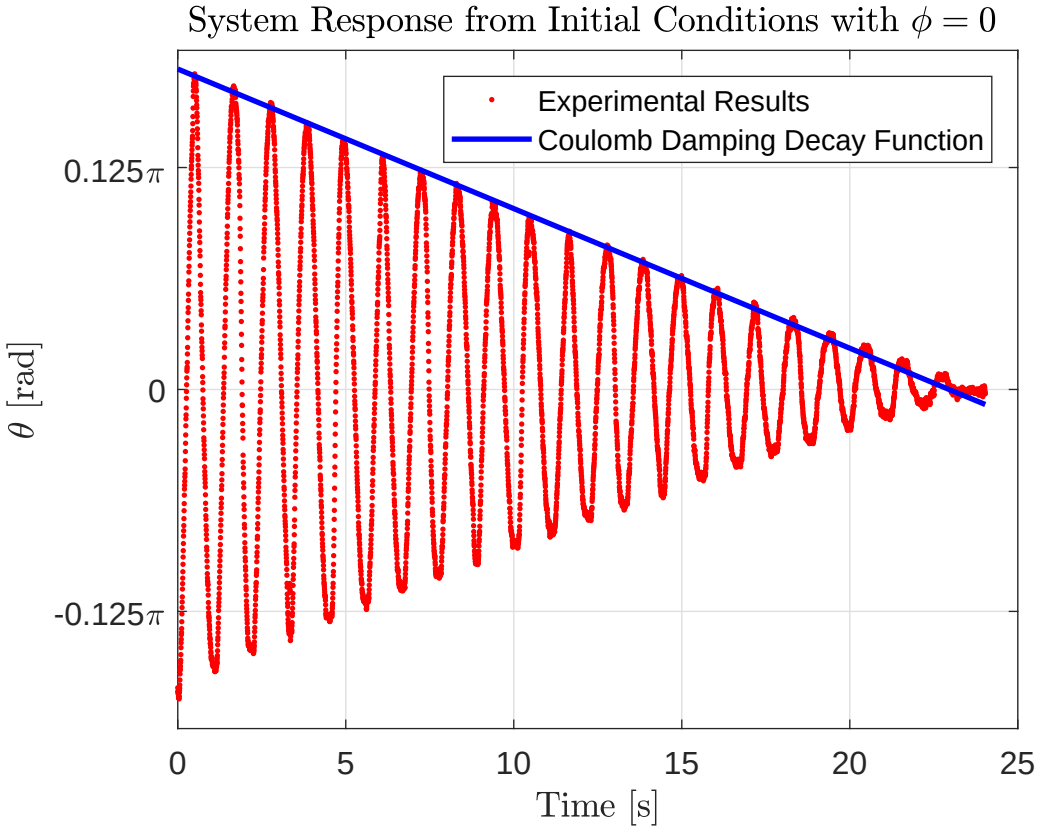

Figure 2.3: Initial Condition System Response while $\phi = 0\,\mathrm{rad}$

The second natural frequency was determined by analysing the response of the system when ϕ starts at a initial condition and keeping $\theta = 0\,\text{rad}$ throughout the response. This was accomplished by constraining the non-actuated pendulum using hard stops. Figure 2.4 shows the measured response of the system when ϕ starts at a initial condition and keeping $\theta = 0\,\text{rad}$.

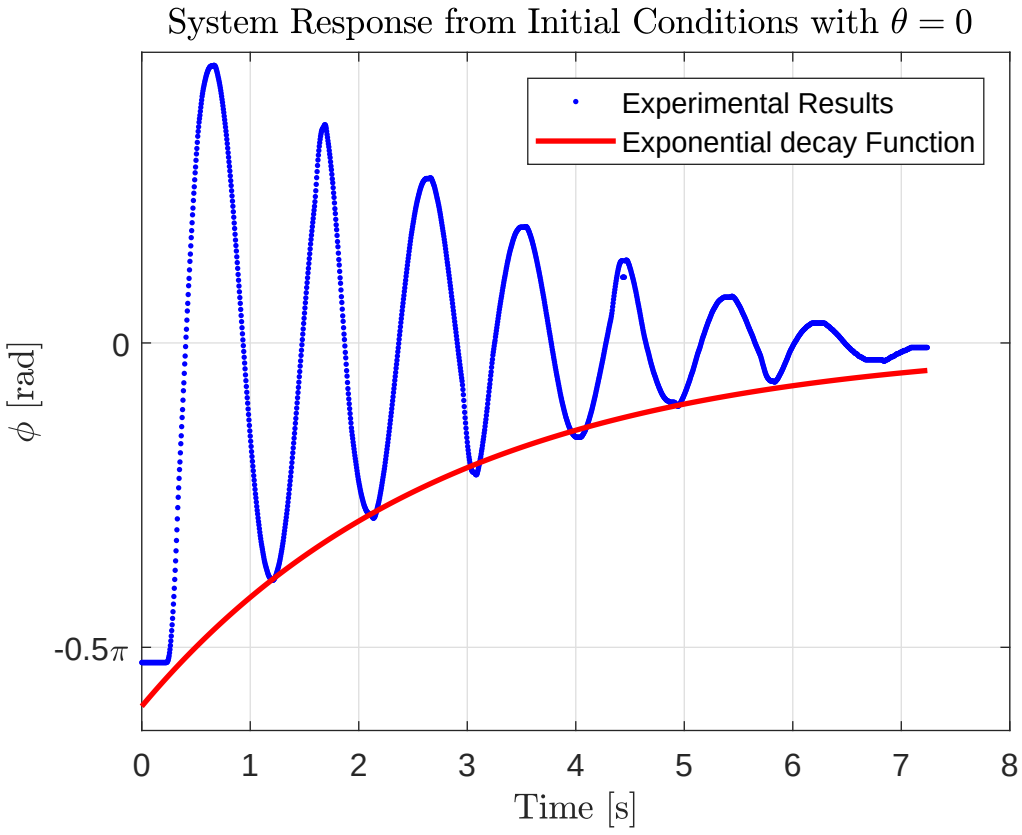

Figure 2.4: Initial Condition System Response while $\theta = 0\,\text{rad}$

The damped natural frequencies of the system were identified by inspecting the frequency content of the time-domain responses. The frequency content of the initial condition responses of both experiments are shown in Figure 2.5, by applying the Fast Fourier Transform (FFT) algorithm to the time-domain signals. The FFT indicates the damped natural frequencies by the predominant peaks across the frequency spectrum which are tabulated in Table **??**.

The response shown in Figure 2.3 is under the influence of coulomb damping due to the response being characterised by the amplitude decaying linearly with a constant slope. Coulomb damping is caused by sliding friction and it's force is opposite to the direction of velocity (Inman, 2015). It is thus characterised

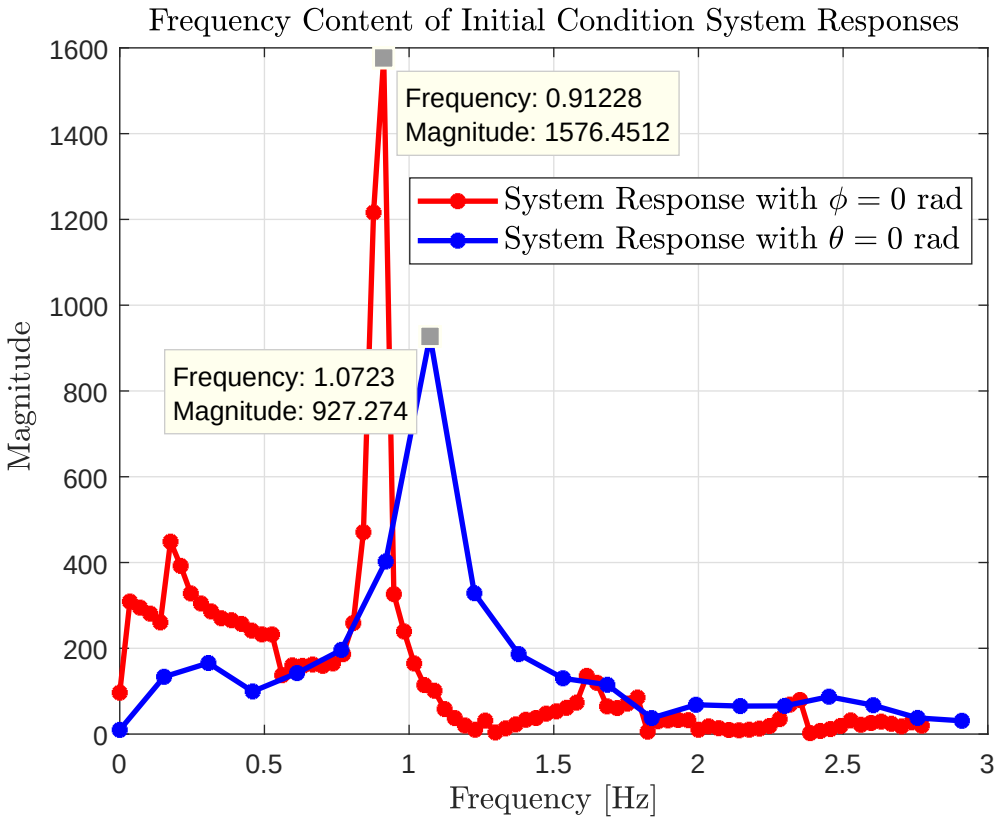

Figure 2.5: Frequency Content of Time-Domain Initial Condition Responses

as

$$f_{c_1} = \left\{ \begin{array}{cc} -\mu N & \dot{\theta} > 0 \\ 0 & \dot{\theta} = 0 \\ \mu N & \dot{\theta} < 0 \end{array} \right\}$$

It is shown in Inman (2015) that the slope is defined as

$$-\frac{2\mu N \omega_n}{\pi m g} \tag{2.13}$$

where N is the normal force. The slope seen in the decay function in Figure 2.3 was calculated using linear regression and by knowing the terms in equation 2.13 the combined μN term can be calculated and is shown in Table **??**.

The responses shown in Figure 2.4 can be modelled as a second order differential equation of the form:

$$\ddot{\phi} + 2\zeta\omega_n\dot{\phi} + \omega_n^2\phi = 0$$

System	ω_{n_1}	ω_{n_2}	ζ_1	ζ_2
Experimental	5.692	6.793		
Simulation	5.654	6.704		

Table 2.2: Experimental Characteristics vs Simulation Model Characteristic

. The amplitude is seen decaying exponentially with time and this behaviour is be modelled by the following equation:

$$\tau(t) = Ae^{-\zeta\omega_n t}$$

where ω_n is the natural frequency, ζ the damping ratio of the system and A represent the initial condition. The damped natural frequencies of the system has already been determined and linear regression was used to determined the best ζ that will fit the measured data. The decaying function is shown in Figure 2.4 with the ζ value shown in Table **??**. It is visible from the response that the damping ratio fits the data well and only starts to deviate near steady state.

The damping force, f_{c_2} that develops between the stator and rotor of the hinge can then be characterised as $2\zeta\omega_n(\dot{\phi} - \dot{\theta})$. The subtraction of $\dot{\theta}$ is due to the rotor of the hinge rotating relative to the stator.

2.5 Model Validation

The model implemented in simulation must be able describe the physical model to an acceptable degree to allow any further development on the simulated model. The simulated model will be validated by comparing the experimental system characteristic values to those attained in simulation.

Table 2.2 shows the experimental values determined in the previous section against the simulation characteristic and indicates the simulation model represents the physical model well. Figure 2.6 and **??** provides an visually verification that the damping effects are modelled to an acceptable degree.

The proof presented indicates the physical model is well represented and further developments on the simulated model may occur.

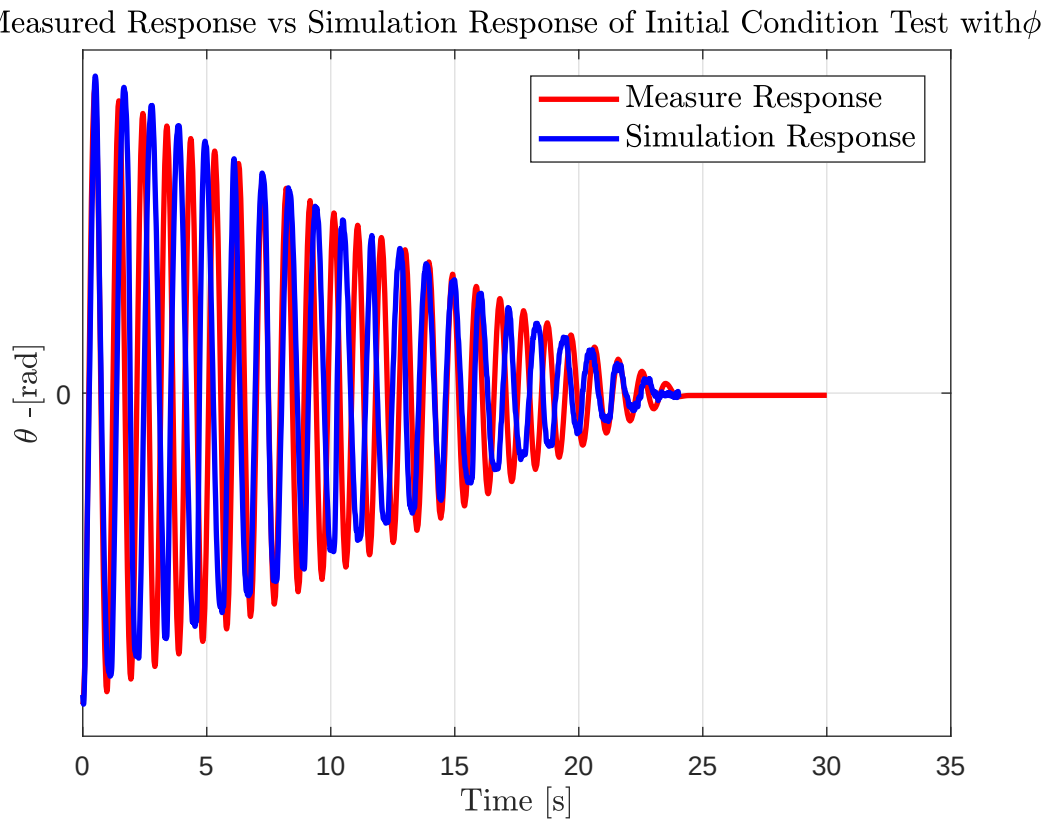

Figure 2.6: Comparison between Simulated and Measured Response

Chapter 3

Feedback Control Design

3.1 Balancing Controller

Provided the robotic gymnast is in the vicinity of the unstable equilibrium position, a balancing controller is required to balance the system in the inverted position. The design approach was based on the premise that the swing-up controller will swing the robotic gymnast to the vicinity of the unstable equilibrium position where the balancing controller will take over. This section will focus on the aspects required to implement this balancing controller.

3.1.1 Controller Architecture

Figure 3.1 shows the block diagram that implements the balancing controller, and it is clear that the state space representation of the system was used. This requires the system to be a linear time invariant (LTI) system, but the system describe in equation (2.3) and (2.4) are not linear. This requirement was satisfied by linearising the system.

Another aspect of the balancing controller is that there are no reference input to instruct the controller to guide the robotic gymnast to the unstable equilibrium position. This is due to the system being linearised at the unstable equilibrium position and results that the unstable open-loop poles describe the

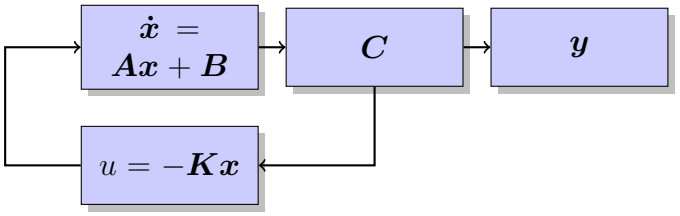

Figure 3.1: State Space Representation of the Balancing Controller

system response from initial conditions from the inverted position. Feedback is used to move these poles to stable locations and results in the closed loop system to decay to the unstable equilibrium position from initial conditions around the inverted position.

3.1.2 Requirements/Specifications and Constraints

The requirements set out for the balancing controller were to bring the robotic gymnast to the unstable equilibrium position from an initial condition range of:

$$\vec{q_i} = \left\{ \begin{array}{c} \theta > \frac{\pi}{1.1} \, \Lambda \, \theta < \frac{-\pi}{1.1} \\ \phi > \frac{\pi}{12} \, \Lambda \, \phi < \frac{-\pi}{12} \end{array} \right\}$$

The response must have a settling time of 0.8 seconds and a percentage overshoot M_p of 5%.

These requirements was selected to give the swing-up controller enough margin to bring the system to the vicinity of the unstable equilibrium position where the balancing controller is capable of balancing.

3.1.3 Plant Linearisation

As mentioned previously, to implement the state space representation the system must be a LTI system. This was achieved by using the Taylor Series Expansion to linearise the system at the unstable equilibrium position.

The independent parameters, ϕ and θ, will be condensed from now on as a vector describes as

$$\vec{q} = \begin{bmatrix} \theta \\ \phi \end{bmatrix}$$

The system is linearised at

$$[\vec{q_s}, \dot{\vec{q}_s}, \ddot{\vec{q}_s}]^T = [\pi, 0, 0, 0, 0, 0]$$

with the mathematical details shown in Appendix A.3. This linearised model can then be written in the state space form to implement a feedback gain. The state space variables are chosen as $\Delta\vec{q}$ and $\Delta\dot{\vec{q}}$ which results in the state space representation as:

$$\dot{\vec{q}} = \boldsymbol{A}\Delta\vec{q} + \boldsymbol{B}u$$

$$\vec{y} = \boldsymbol{D}\Delta\vec{q} + \boldsymbol{0}u$$

The poles of the system are identified by determining the eigenvalues of the $\boldsymbol{A}$ matrix. The linearised system remains a coupled system which results that the quadratic eigenvalue problem shown in equation (3.1) was required to be

solved to identify the poles. The solved quadratic eigenvalue problem results in the following eigenvalues using the system parameters in Table 2.1.

$$Q(\lambda) = \lambda^2 M + \lambda C + K \tag{3.1}$$

$$\vec{s} = \begin{bmatrix} 10.5742 \\ 4.9498 \\ -11.4905 \\ -5.0215 \end{bmatrix}$$

The eigenvalues of the system are all real indicating the response of the system when disturbed is an exponential function. This can be explained by realising the linearised system is modelled as a single pendulum. Once the single pendulum is disturbed from the unstable equilibrium position it would continue to rotate downwards and not with an oscillatory response.

3.1.4 Full State Feedback Design

The poles of the system are pairs of positive and negative real poles that indicate an unstable system. This is expected due to the system being linearised at the unstable equilibrium position. When the linearised system is at rest, any disturbance will result in a theoretically infinite growth of the state variables, but this behaviour can be controlled by introducing feedback.

These poles will be moved to the desired position by using the method of dominant poles. The method of dominate poles chooses a pair of the poles for the closed-loop system and select the other open-loop poles to have real parts with much larger natural frequencies. This allows the higher-order system response to be characterised as a second-order response Gene F. Franklin (2015).

Assuming a second order system and using the requirements defined, the pole locations can be calculated using equation (3.2) and (3.3)

$$M_p = \exp(\frac{-\pi\zeta}{\sqrt{1-\zeta^2}}) \tag{3.2}$$

$$t_s = \frac{4.6}{\zeta\omega_n} \tag{3.3}$$

and knowing the poles are described seen in equation (3.4)

$$p = \zeta\omega_n \pm j\omega_d \tag{3.4}$$

results in the desired pole locations as:

$$\vec{p} = \begin{bmatrix} -5.7500 + j5.8662 \\ -5.7500 - j5.8662 \\ -24.6429 \\ -24.6429 \end{bmatrix}$$

3.1.5 Simulation Response

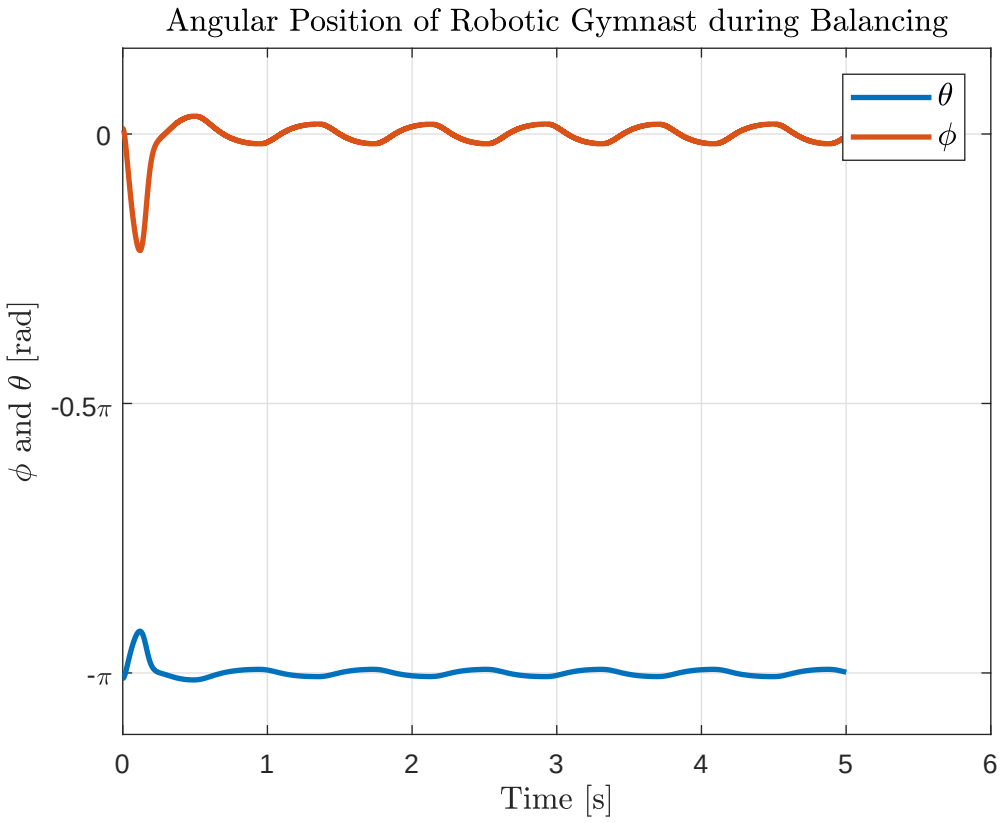

Figure 3.2: Balancing of the Robotic Gymnast

Figure 3.2 shows the robotic gymnast balancing around the unstable equilibrium position from an initial condition of

$$\vec{q} = \begin{bmatrix} \frac{\pi}{0.1} \\ \frac{\pi}{10} \end{bmatrix}$$

The oscillatory response around the inverted position is due to the non-linear coulomb damping that was approximated as viscous damping. This oscillatory response was decided to be acceptable due to the assumption that the effect of coulomb damping is negligible at low velocities. This assumption is visible

in Figure 2.3 where the response depart from the linear decay function near the stable equilibrium position.

The response shows that the controller meets the requirement of balancing the robotic gymnast from initial condition of $q \in []$ and reaches steady state within 0.8 seconds. The overshoot requirement of

3.2 Swingup Controller

For the robotic gymnast to swing from the stable equilibrium position to the unstable equilibrium position the feedback control must incorporate the non-linearities of the system. How these non-linearities of the system are incorporated and the design approach to swinging will be explained in the following section.

3.2.1 Controller Architecture

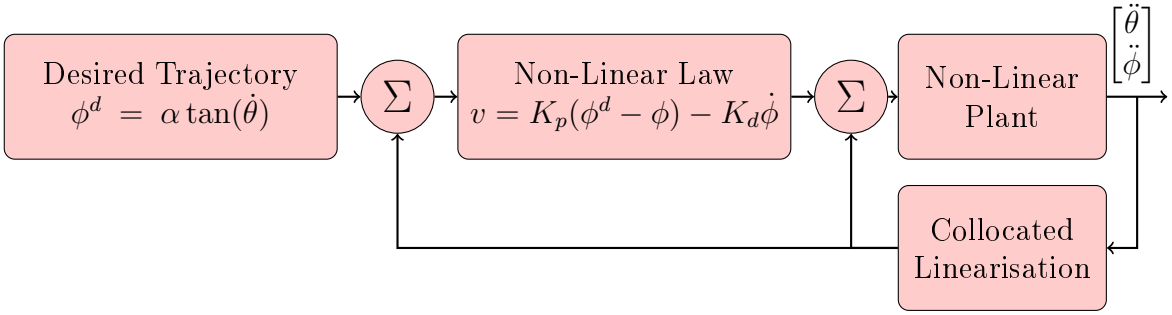

Figure 3.3: Block Diagram of the Non-Linear Controller

Figure 3.3 shows a high-level block diagram of the multiple parts of the swing-up controller. These parts are required to work in unison to allow the robotic gymnast to swing.

The collocated linearisation block is the foundation on which the entire controller was built. It creates a linear response from one of the outputs of the plant. This linear response can then be used to follow a desired trajectory.

The swing-up controller implements classical control theory approach where gains are selected to characterise the response of the system based on the error of the desired trajectory and the actual trajectory of the system.

Each of the blocks shown in the block diagram will be discussed in the section below.

3.2.2 Requirements/Specifications and Constraints

The requirements of the swing-up controller is to swing the robotic gymnast up under 30 seconds in the vicinity of the unstable equilibrium position. The vicinity of the unstable equilibrium position is defined as $\theta = 2\pi\,\text{rad} \pm \frac{\pi}{30}$ and $\phi \in [-5°, 5°]$.

Constraints that are placed on the controller are not to use 50% of the stall torque of the motor during the entire swing-up of the robotic gymnast.

The first requirement is to provide a feasible solution to the swing-up of the robotic gymnast and allow the swing-up sequence to be captivating. The second requirement is to ensure the linear approximation of the system is acceptable when the balancing controller is active to bring the system to the inverted position and balance. The constraint placed was to increase the safety in testing and prolong the life of the motor.

3.2.3 Feedback Linearisation

It has been shown that it is not possible to linearise the dynamics of the gymnast by means of static state feedback and non-linear transformation mur (1990), but it is possible to achieve a linear response from one of the outputs of the plant by implementing a non-linear feedback. This non-linear feedback is the partial feedback linearisation.

Collocated linearisation is a form of partial feedback linearisation where a non-linear control input τ is used to linearise the response of the actuated pendulum $\ddot{\phi}$. By analysing equation (2.4), the input τ was chosen to cancel all the non-linearities of the system and add an additional outer loop control input v_2 as seen in equation (3.5). This results in the non-actuated pendulum to see a indirect force and the problem can be reduced to finding the outer loop control input to force the actuated pendulum to swing upwards (spo, 1995).

The derivation of the collocated linearisation is shown in Appendix **??**.

$$\tau = d_{21}\ddot{\theta} + v_2 d_{22}\ddot{\phi} + h_2 + \psi_2 \tag{3.5}$$

$$d_{11}\ddot{\theta} + h_1 + \psi_1 = -d_{12}v_2 \approx F \tag{3.6}$$

$$\ddot{\phi} = v_2 \tag{3.7}$$

The subtle practical implication of using collocated linearisation is that the system being controlled must be well defined. If this is not the case the non-linear input τ will introduce other unwanted dynamics that could lead to undesirable behaviour.

3.2.4 Nonlinear Control Law

The ability to control the actuated pendulum to follow a desired trajectory, provides the possibility to increase the energy of the system if the correct trajectory is chosen. The increase of energy in the system will cause the pendulums to rise from their stable equilibrium position and start swinging upwards. The desired trajectory for ϕ was chosen as equation (3.8) determined by W.Spong in (spo, 1995).

$$\phi^d = \alpha \arctan(\dot{\theta}) \tag{3.8}$$

This desired trajectory was derived by analysing a single pendulum and approximating the force it experience as seen in equation (3.6). By using this approximation W.Spong shows in spo (1995) that the desired trajectory will increase the energy in the system. The desired trajectory also tries to allow the actuated pendulum to swing in phase with the non-actuated pendulum and by this approach the energy of the actuated pendulum is transferred to the non-actuated pendulum (spo, 1995).

The outer loop control input, v_2, then implements the classical control approach where gains are selected to characterise the response of the system based on the error seen in equation (3.9)

$$v_2 = K_p(\phi^d - \phi) - K_d\dot{\phi} \tag{3.9}$$

The coefficient α used in equation (3.8) constrains the actuated pendulum to stay within a interval of $\phi \in [-\beta, \beta]$ where $\alpha < \beta$ (spo, 1995). This provides better control over the system to stay within the null controllability region when the system reaches the unstable equilibrium position.

Another side-effect of using the non-linear controller is that at rest the system will not start to swing-up. At rest, the condition are: $\phi = 0\,\text{rad}$ and $\dot{\phi} = 0\,\text{rad/s}$, and results that the control output seen in equation (3.9) will be zero. This effect was overcome by giving the system a small initial condition to start the swing-up controller.

3.2.5 Simulation Response

Figure 3.4 shows the swing-up controller swinging the robotic gymnast from the stable equilibrium position to the vicinity of the unstable equilibrium position. There are a few interesting occurrences in the responses that were mentioned in the previous section to bring the reader's attention.

Firstly the robotic gymnast is required to start at an initial condition for the swing-up control law to be active and this is seen with θ starting 11°.

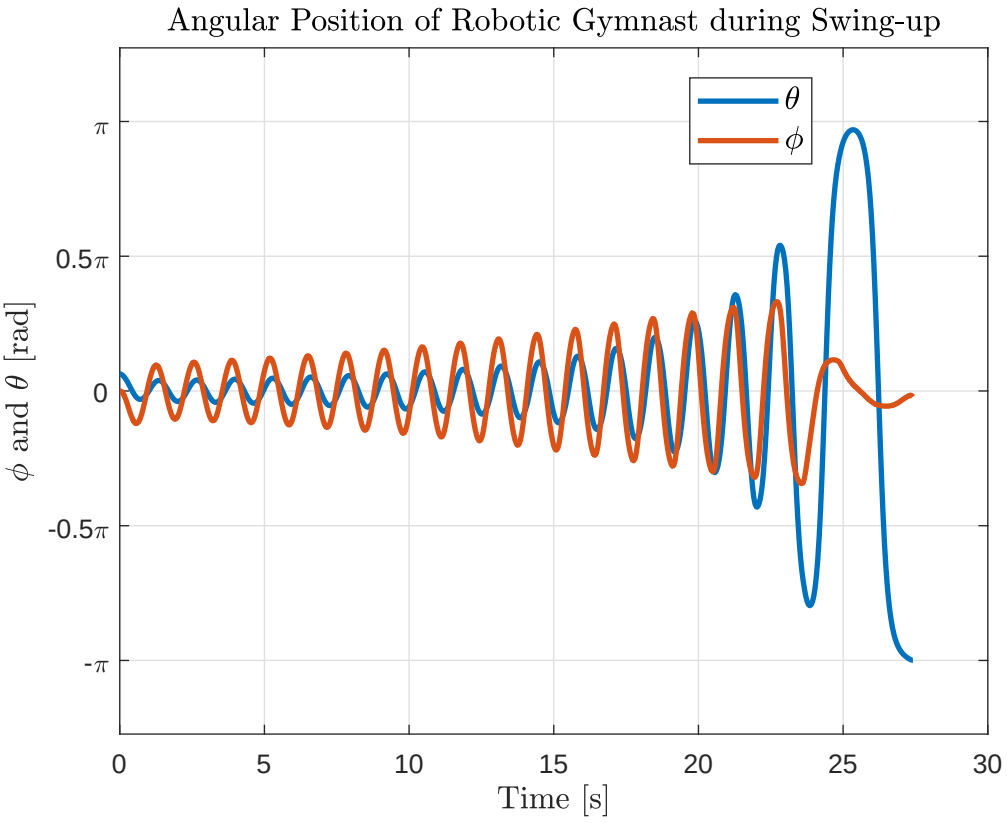

Figure 3.4: Swing-up of the Robotic Gymnast

Secondly the amplitude of ϕ is seen to suddenly decrease when the system nears the inverted position. This is due to α being reduced when the robotic gymnast nears the inverted position.

The response shows the swing-up controller meets the designed requirements by swinging the robotic gymnast to the vicinity of the unstable equilibrium within 30 seconds and θ and ϕ are in the designed region for the balancing controller to bring the system to the inverted position.

3.3 Simulation Results

Once both controllers were capable of meeting the requirements set out, they needed to be combined to achieve the swing-up and balancing of the robotic gymnast. Figure 3.5 shows the response of both controllers combined that achieved the swing-up and balancing.

During the swing-up the α value was reduced as the robotic gymnast started nearing the unstable equilibrium position as seen below.

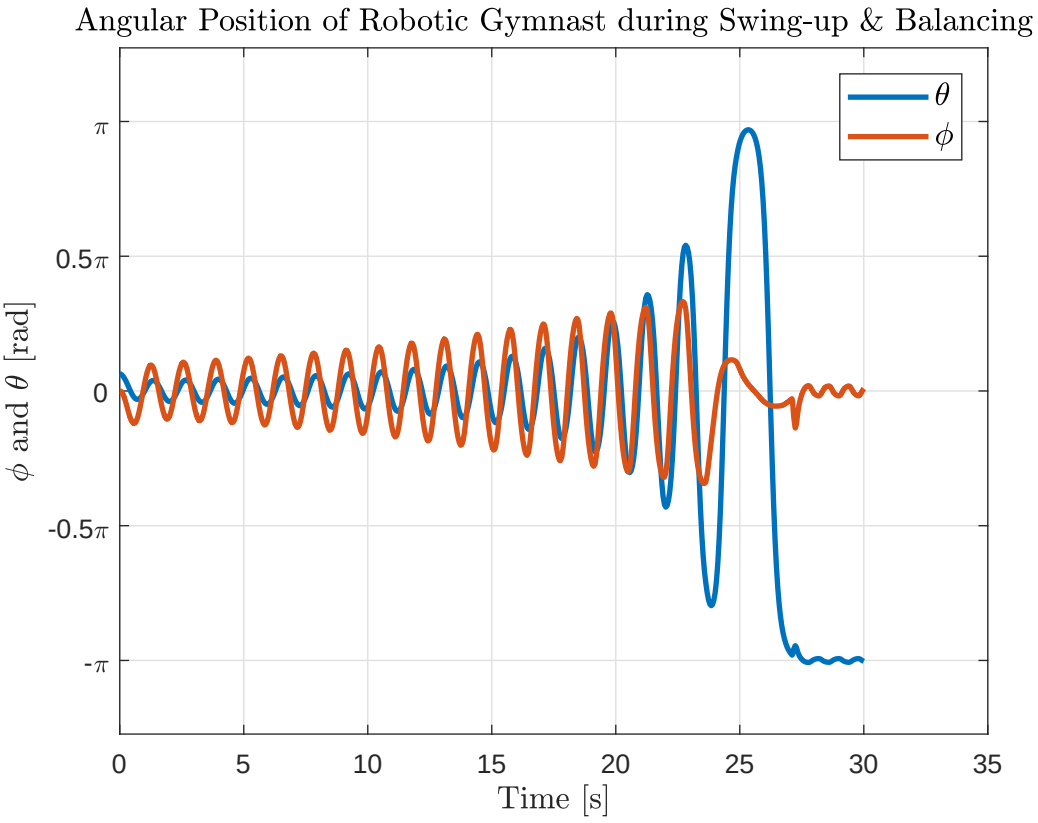

Figure 3.5: The Swing-Up & Balancing of the Robotic Gymnast

$$\alpha = \left\{ \begin{array}{ll} \frac{\pi}{2} & \frac{-\pi}{2} < \theta < \frac{\pi}{2} \\ \frac{\pi}{12} & \\ \frac{pi}{24} & \frac{-\pi}{1.1} > \theta\theta > \frac{\pi}{1.1} \end{array} \right\}$$

Chapter 4

Hardware Design and Implementation

4.1 Mechanical Hardware

The mechancial design that created the physical model is presented here. The physical model allowed the abstract mathematical model to be implemented and experiments to be conducted. It will be presented by discussing the various components required and design decision made to implement a physical model that represents the mathematical model.

Figure ?? shows the physical model designed and used for experiments. It emphasises some of the more critical components that were required.

It is important that the physical model holds the assumption made during the derivation of the robotic gymnast. These assumptions include planar dynamics of the robotic gymnast and rigid body dynamics. The assumption of planar dynamics comes in affect with the connection between the rotating shaft and the non-actuated pendulum. If the assumption holds there should be no vibration of the pendulum in any other direction than the rotating plane of the pendulums.

The assumption of rigid body dynamics is easily met due to the forces acting on the pendulums results in negligible strain and elongation can be ignored.

4.1.1 Mechanical Components

The components emphasised in Figure ?? are discussed in the following section and explains their significance of use.

The electrical slipring converts the rotating wires that lead to the motor mounted on non-actuated pendulum to stationary wires allowing for free rotation and easy connection to the electrical design.

The bearing housing holds the ball-bearings in place ensuring for no unwanted vibration and misalignment. These ballbearings were press-fitted into the housing, ensuring a secure connection.

The potentiometer's shaft is connected to the shaft by means of a rubber tube. The rubber tube was chosen due to easy connection, allows for misalignment and the delay of measurement due to elasticity of the rubber is negligible.

The non-actuated pendulum is connected to the shaft by means of using 3 screws. The diameter of the shaft was kept as small as possible to reduce the inertia and friction. This method of connection was deemed the best to achieve the diameter used.

4.1.2 Structural Force Analysis

Little calculation were done to determine whether sizes chosen for the diameters of the shaft were capable of withstanding the loads. Reason being based on experience that the chosen diameters are more than enough capable of withstanding the loads. The following section will provide the proof that the selected diameters are able to carry the loads.

The shaft was modelled as a simple supported beam with the diameter being the smallest used in the actual design. This model is conservative due to the design being a supported by 3 distributed reaction forces. Figure 4.1 shows the conservative model.

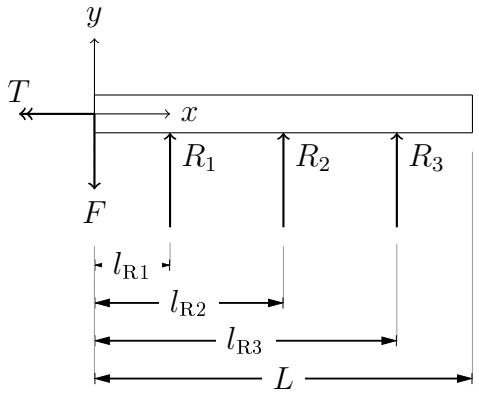

Figure 4.1: Model of Rotating Shaft as a Simplified Beam

The equations () and (4.2) shows the maximum axial- and torsion load the beam will experience with the configuration shown in Figure 4.1 (reference shigley). The principal stresses in the shaft was than determined through equations () and () (reference). Using the conservative Von Mises yield criteria shown in equation (4.3) the safety factor on static yielding was determined using the constants defined in Table XXX.

$$\sigma_f = \frac{F \cdot l_r}{I} \tag{4.1}$$

$$\tau_f = \frac{T \cdot r}{J} \tag{4.2}$$

$$n_s = \frac{\sigma_v}{\sigma_2} = \sqrt{\frac{1}{2}[(\sigma_1 - \sigma_2)^2 + (\sigma_2 - \sigma_3)^2 + (\sigma_3 - \sigma_1)^2]} \tag{4.3}$$

The shaft will experience cyclic loading due to the rotation.

4.1.3 Inertia of Pendulums

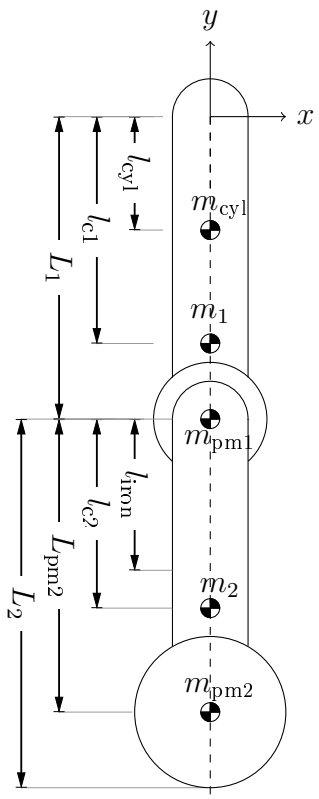

Figure 4.2: Simplified Drawing of Physical Model

Figure 4.2 shows a functional drawing of the physical model to visually aid the reader in understanding how the inertia of the system was determined. In equation (2.3) and (2.4) the I_a and I_b represents the inertia of the non-actuating and actuated pendulum about the axis coming out of the page passing through their center of mass respectively.

Each pendulum contains many parts that contribute to their inertia due to each part representing a different physical form. How the inertia values shown in Table 2.1 were determined will be shown below with the physical system parameters shown in the Table 4.1

The actuated pendulum consist out of an aluminium square rod connected to the shaft and the motor mounting. The inertia of a square rod through it's center of mass is:

$$I_{cyl} = \frac{1}{12} m_{cyl}[w^2 + L_1^2]$$

The motor, gearbox and the motor mount was viewed as a point mass. It's inertia around the center of mass of the non-actuated pendulum is:

$$I_{pointmass_1} = m_{pointmass_1} \cdot [L_1 - l_{c1}]^2$$

The total inertia of the of the non-actuated pendulum is then:

$$I_a = I_{pointmass_1} + I_{cyl} + m_{cyl} \cdot [l_{c2} - l_{cyl}]^2$$

The actuated pendulum contains similar parts as the non-actuated pendulum. A pointmass at the bottom and an iron rod connected to the motor shaft and the pointmass. Determining the inertia is thus exactly the same as the non-actuated pendulum.

During the simulation it was noticed that the ratio between the unactuated and actuated pendulum should be 1 or greater for the swing-up controller to bring the robotic gymnast to the unstable equilibrium position in a feasible time frame. This is the reason behind adding another point-mass to the actuated pendulum to compensate for the inertia the motor creates as a point mass.

4.1.4 Center of Mass

Each pendulum can be seen as a system containing discrete components, where each components center of mass is easily identified. Both iron rod and aluminium rod center of mass is in the middle of their rod lenght and the rest are seen as point masses. However each of these components center of mass contribute to the center of mass of each pendulum.

Non-Actuated Pendulum	Value	Actuated Pendulum	Value
m_{cyl}	5	m_{iron}	
w_{cyl}	3.3	w_{iron}	
$m_{\text{pointmass1}}$	12	$m_{\text{pointmass2}}$	
l_{cyl}	12	l_{iron}	
L_{c1}	12	L_{c2}	
L_1	12	L_2	

Table 4.1: Physical Model Paramaters

Pendulum	Center of Mass [m]
Non-Actuated	0.2056
Actuated	0.2115

Table 4.2: Center of Mass for Each Pendulum from their Rotating Hinge

The center of mass for each pendulum from their hinge of rotation shown in Table 4.2 was calculated using equation (4.4).

$$\vec{r} = \frac{\sum_i^j r_i m_i}{\sum_i^j m_i} \tag{4.4}$$

4.1.5 Motor

The chosen motor used during experiments was the *Faulhaber DC 3257 012 CR* micromotor. It was used in combination with the *Faulhaber Planetary Gearhead 32/3* Series. The gearbox is a 2 stage reduction gearbox with a overall rounded reduction ratio of 14:1. The motor is capable of providing a stall torque of 539 mNm which is a converted output torque from the gearbox of 7.646 Nm.

The motor terminal connection is connected directly to the PCB of the electronic design being routed through the slipring. The motor assembly contains a encoder for position measurements and it's signal and power connection is also routed through the slipring and connected to the PCB.

4.1.6 Assembly

4.2 Electronic Hardware

The electronic hardware was a crucial component for the successful implementation of the robotic gymnast. The electronic design provided the means to determine the system characteristic and verification of the simulated model. It

will be presented by discussing the various components implemented to achieve the results in this report.

4.2.1 System Description

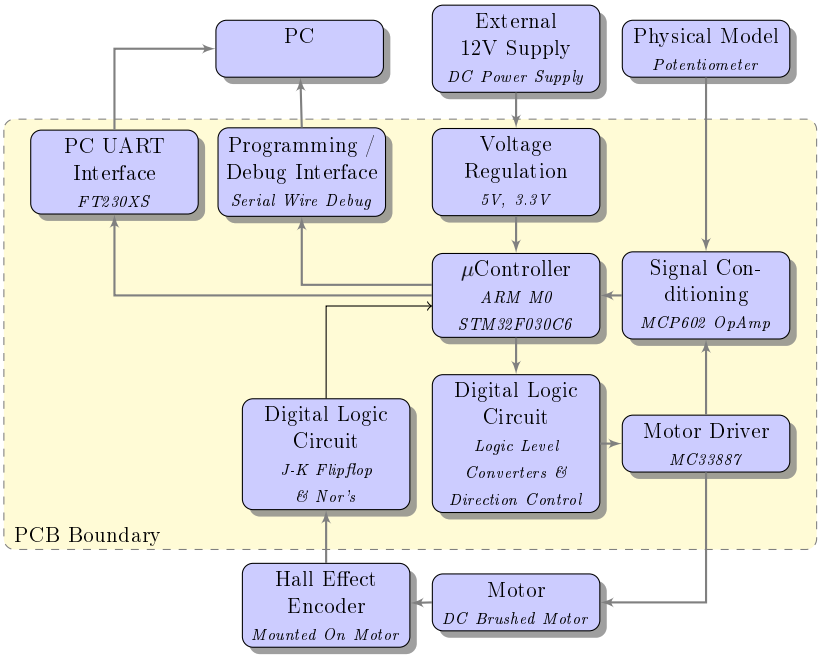

Figure 4.3: Electronic System Overview

Figure 4.3 provides a system overview on how the different subsystems functions together and what inputs are outside from the PCB design.

The micro-controller receives the different signals that has been correctly conditioned from supporting circuitry to interpret the dynamics of the system. From these signals it is able to output the correct signals to instruct the next command to the motor.

The digital logic circuit that consist of logic level converters acquires the signal from the micro-controller and performs signal conditioning to interface with the motor driver and determines the correct direction to rotate the motor.

The motor driver controls the DC brushed motor based of the digital signals and provides a proportional feedback current that is delivered to the unity-gain amplifier.

The motor contains an encoder that indicates the direction and position of the rotor through digital signals that is sent through a digital logic filter to

retrieve only critical information from the encoder signals.

The physical model contains a potentiometer that measures the non-actuated pendulum's angle and this signal is sent to the unity-gain amplifier.

The microcontroller will use the UART interface as it's data acquisition protocol to send the necessary information to the computer.

The micro-controller is programmed using the Serial Wire Debug (SWD) protocol to transfer the binaries from the computer.

Power is provided using a external 12V power-supply, which will power the motor, but also using a regulator to down convert/step to a 5V and 3.3V to power the microcontoller and the other peripherals.

4.2.2 Microcontroller

The microcontroller chosen is the STM32F030Mxx. The selection was done according to the ease of setting up, memory size, physical dimensions and the peripherals it provided. These selection are expanded below.

The STM32F030MXX is based of the ARM M0 architecture which is ARM's entry level micro-controller. It requires little support circuitry to have a up and running micro-controller with only the SWD protocol to program the chip.

It was difficult to determine the memory size specification for the project. This uncertainty ensured that the largest memory size the ARM M0 architecture could provide was selected.

The Electrical and Electronic Department's Printed Circuit Board (PCB) manufacturing machine can only provide a minimum track width 0.3 mm. This resulted in choosing a microcontroller whose footprint would meet this requirement.

Based on the conceptual design, the chosen microcontroller required to contain 2 ADC's channels, minimum of 5 GPIO's and 1 serial communication peripheral.

4.2.2.1 Programming / Debug Interface

The *Atollic TrueSTUDIO for ARM 8.0.0* Integrated Development Environment (IDE) was used for writing the source code which converts the source code to the Executable and Linkable Format (.elf) file. These .elf files is then written using the SWD protocol to the micro-controller. Debugging of the

Component	Supply Voltage [V]
Digital Logic, Op-Amp & Sensors	5
Microcontroller	3.3
Motor Driver	12

Table 4.3: Suppy Voltage's for the different components

source code occurred using the same IDE which allows the programmer to inspect variables, timers and logic.

4.2.2.2 PC UART Interface

The purpose of the UART to serial communication was for data acquisition of the system response and for debugging.

The UART to serial communication was implemented due to the external computer executing a Python script listening for any activity on the computer's driver port for information about the system.

The UART to serial communication was also used for debugging the system. Special instruction from the Python script could be sent to verify correct sampling of signals, manual control over the duty-cycle of the PWM signal and directional control of the motor. It also acted as a soft layer for safety by sending commands to arm the system before experiments.

The UART to Serial chip used was the FT230x (USB to BASIC UART IC). It was chosen due the easily support circuitry it requires with the option to use LED's to indicate any activity on the receive (Rx) & transmit (Tx) communication lines.

The UART to serial circuit was tested by doing a loop-back test. The loop-back test consist of connecting the Tx and Rx lines together. This results in the circuit echoing anything back to the receiver. The schematic of the circuitry is shown in Appendix A.5.

4.2.3 Voltage Regulation

The various components used in the electronic design required different supply voltages and are tabulated in Table 4.3.

The 12 V supply was provided using an external bench power-supply. The 5 V and 3.3 V was provided using linear voltage regulators for each voltage. The schematic for each voltage regulator are shown in Appendix A.5, where each voltage regulator circuit includes a Light Emitting Diode (LED) to ensure

the minimum load was met for each regulator. The LED also acts as a visual debugging method.

4.2.4 Potentiometer Sensor

4.2.4.1 Working Principle

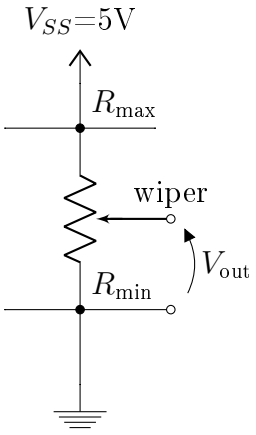

Figure 4.4: Simplified Model of a Potentiometer

The rotary position potentiometer consist out of a wiper that is attached to a rotating shaft. This wiper moves across a internal resistor as the shaft rotates and changes the effective resistance across the output terminal. It provides thus a proportional voltage to it's position as seen in Figure 4.4 that indicates the position.

4.2.4.2 Interface

The signal produced by the rotary potentiometer varies from 4.95V and 50mV as it rotates from 360° to 0°. This signal is sent through a simple voltage divider circuit to reduce the signal to 3V and 15mV to be within the sampling limits of the micro-controller. The scaled voltage is then sent through a unity gain rail-to-rail amplifier, where the mirrored output signal is fed into the ADC.

The type of ADC used in the STM32F030XX is a successive approximation register (SAR) and contains an internal capacitors that suffers from the effect of being depleted if the sampling frequency is to high (stm, 2017). Using an operational amplifier reduces the risk of depleting this internal capacitor because of the low output resistance. The schematic of the circuit is shown in Appendix A.5.

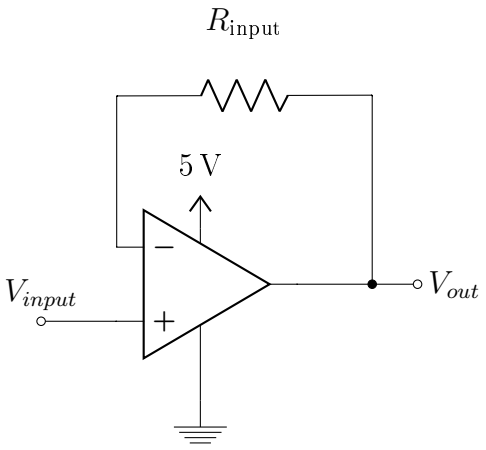

Figure 4.5: Unity Gain Amplifier Circuit

4.2.5 Magnetic Encoder

4.2.5.1 Working Principle

A rotating gear containing ferrous metal teeth is attach to the rotating shaft. The rotating metal teeth rotates near a hall-effect sensor which creates a change in the magnetic flux inside the hall-sensor. This change in magnetic flux is sensed by the hallsensor which produces a digital signal (Instruments, 2006).

4.2.5.2 Digital Interface

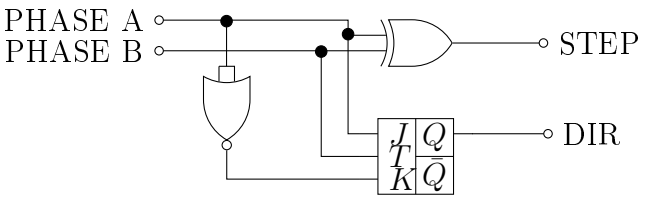

Figure 4.6: Digital Logic Circuit containing JK-Flipflops, XOR- and NOR Gates

The encoder contains a sold state hallsensor which provides 2 channels with a 90° phase difference between the them. (Faulhaber, 2011). These 2 signals under go a hardware filter that produces 2 signals that indicate the direction of the motor and the incremental position.

The hardware filter consist out of XOR, NOR and JK-Flipflop gates shown in Figure 4.6 and the schematic is in Appendix A.5. The XOR gate produces the incremental change of position of the motor which is then read by the microcontroller using interrupts on rising and falling edges. The output of the

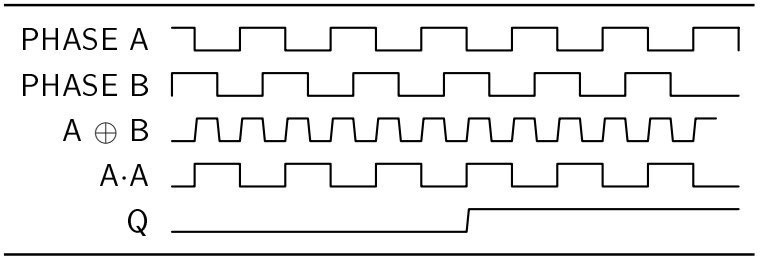

Figure 4.7: Waveform of the JK-Flipflop,XOR, and NOR Gate Circuit

XOR gate is shown in Figure 4.7.

The resolution of the encoder is 16 lines per revolution per channel, equalling to a combined 64 rising- & falling edges in total. The encoder is connected directly to the motor shaft whose speed is reduced by the 14:1 reduction gearbox. The encoder will thus rotate 14 times per output shaft revolution, increasing the resolution to 896 edges per revolution.

The NOR and JK-Flipflop combination produces the direction of the motor by determining whether phase A leads or lags phase B by 90°. This leading or lagging is indicated by a logical 1 or 0 which is read by the microntroller shown in Figure 4.7.

The hardware filter was implemented to reduce the processing time the micro-controller was required to do retrieve the information in the 2 signals.

4.2.6 Motor Driver

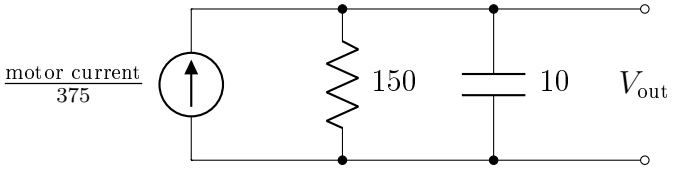

Figure 4.8: Simplified Circuit of Motor Feedback

The motor driver chosen is the MC33887. It was selected based on providing the motor up to 6A of current, while withstanding the high current transients due to the fast switching of a inductive load (mot, 2007). The motor driver provides the motor with 12V DC which is externally provided by a DC power supply. The schematic of the motor driver is shown in Appendix A.5.

The motor driver is connected directly to the motor and responsible for directional and rotational control of the brushed DC motor. The motor driver

contains 2 half H-bridges that forms a full H-bridge which are Pulse-Width-Modulated (PWM) to control the speed of the motor and originates from the microcontroller. The selected frequency was 10kHz and is recommended by the manufacturers mot (2007). As discussed previously, the signals' logic level is first converted and then sent through the AND digital filter before the motor driver receives it.

The MC33887 provides a proportional current of $\frac{1}{375}$ of the current flowing through the high-side of the full H-bridge (mot, 2007). This current is sent through a resistor of 150 Ω to provide a voltage signal to represent the current. Due to the motor being controlled using PWM, the current is a periodic impulse signal making it almost impossible for the ADC to sample. This problem was overcome by adding a parallel capacitor to the resistor to create a ripple voltage. This ripple voltage is sent through an unity-gain amplifier as seen in Figure 4.5 before it is sampled by the micro-controller. The R_{input} resistance is the input resistance that the operational amplifier sees and will be the 150 Ω. This closes the feedback loop to implement torque control by the control system.

4.2.6.1 Logic Level Converters

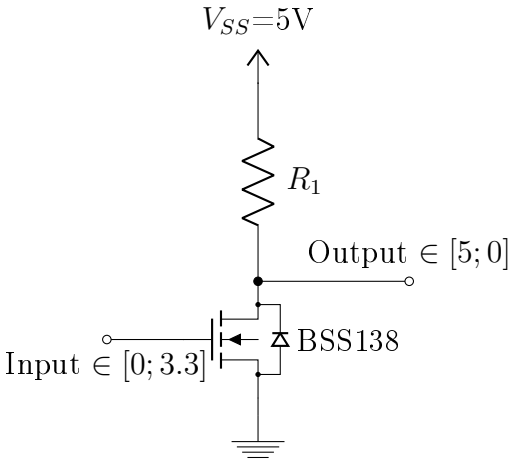

Figure 4.9: Logic Level Converter & Inverter Circuit

The microcontroller is required to interface with the motor driver and represent a logical high and low as a 3.3 V and 0 V respectively. The motor driver's logical high threshold is 3.5 V. It is thus required to use a logic level converter to allow reliable communication between the two devices.

The logic level converter used is shown in Figure 4.9 and uses the BSS128 transistor. The circuit shown also acts as a inverter where a logic low, 0 V by the micro-controller will be converted to a 5 V and a logic high, 3.3 V will be converted to 0 V. This side effect is overcome by inverting the desired responses in software.

4.2.6.2 AND Digital Circuit

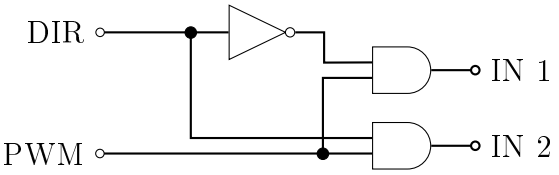

Figure 4.10: AND digital logic with inverter

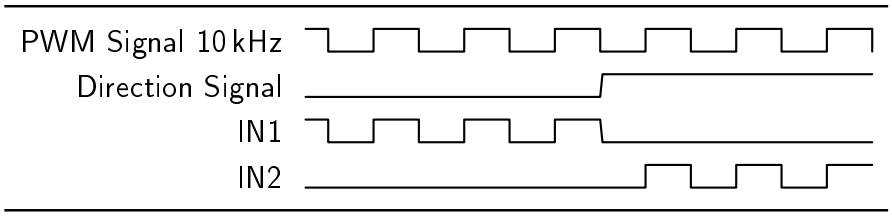

Figure 4.11: AND Digital Logic Circuit Waveforms

The motor driver contains 2 input pins which controls the voltage polarity of the motor terminals. Keeping the one input high and the other low will turn the motor in the one direction and switching the logical values on these inputs will turn the motor on the other direction. Adding speed control requires the PWM signal that the motor receives to be alternated on these inputs and are done by the AND digital circuit.

The AND circuit receives 2 signals from the microcontroller after it has been converted to the correct logic level: the PWM signal and a logic level signal indicating the desired direction. Based on the directional signal the AND circuit will switch the PWM signal between the 2 inputs of the motor driver while holding the other low as seen in Figure 4.11.

This hardware directional control was done in order to reduce the processing time the microcontroller is required to do to switch the generated PWM signal between the 2 inputs of the motor driver.

4.2.7 Verification Tests

4.2.7.1 Angle Sensor Measurements

4.2.7.2 Optical Encoder Measurements

4.2.7.3 PWM Duty Cycle to Motor Current

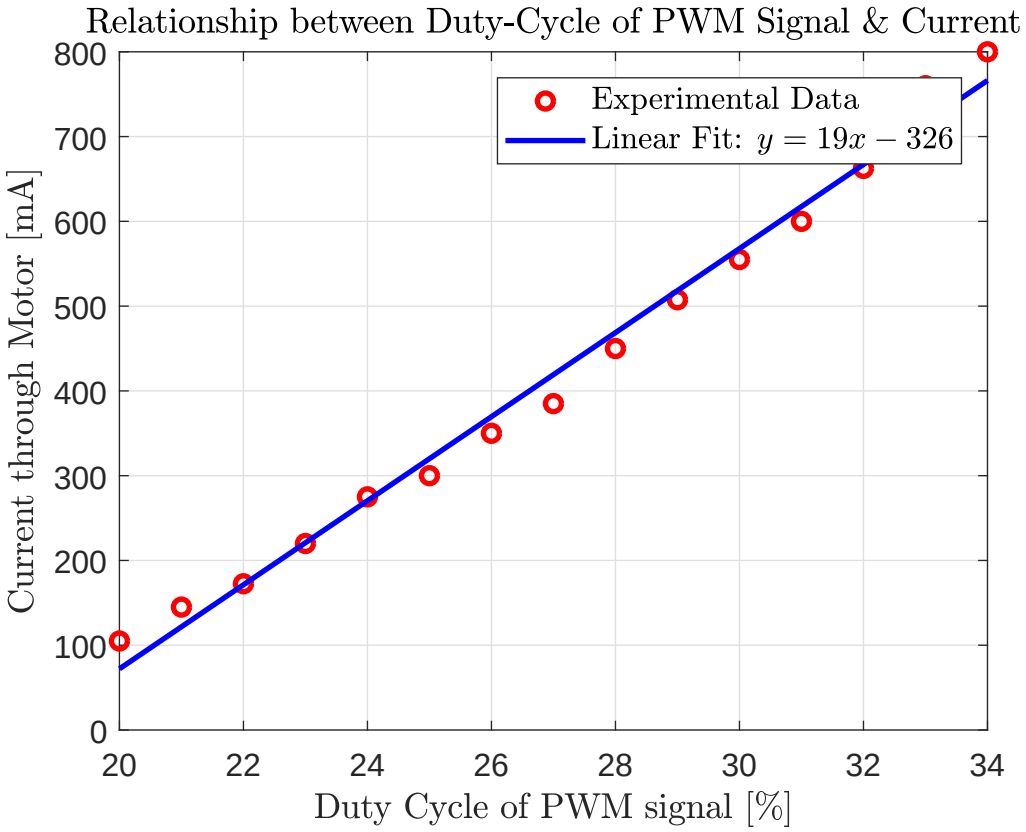

Figure 4.12: Relationship between Duty-Cycle of PWM Signal and Current through Motor

The input to the system is the torque delivered by the motor and the magnitude and direction is determined by the control laws. The model describing the system in equation (2.4) assumes the torque delivered to the system is instantaneously available. This is inaccurate due to the model describing the DC motor is a second-order differential equation containing it's own time-constant. This model was not incorporated due adding another control loop would add more delays to the control systems. To overcome this, the torque provided by the motor would be mapped to the duty-cycle the motor receives.

Experiments were done to determine the relationship between the duty-cycle of the PWM signal and the torque delivered by the motor. These exper-

Constant	Description	Value
GR	Gear Ratio	14
FR	Feedback Current Ratio	375
α_t	Torque Constant	19.1×10^{-3}
R	Resistance	150

Table 4.4: Values of Constants used in Equation (4.5)

iments are done by incrementing the duty-cycle of the PWM signal that the motor receives when the shaft is kept fix against a hard-stop. The mean value of the output voltage from the circuit shown in Figure 4.8 was measured on the oscilloscope and mapped backwards to determine the torque using equation (4.5) with the constants shown in Table 4.4

$$\tau = \frac{V}{R} \cdot GR \cdot FR \cdot \alpha_t \tag{4.5}$$

Figure 4.12 shows the measured data with a line of best fit. It is clear that there exist a linear relationship between the duty-cycle of the PWM signal and the torque provided. This equation of best fit will thus be used to output the correct torque determined by the control system.

Chapter 5

Software Design

The software required to allow data acquisition, retrieval of system state information and communication is presented here. The software design played a central role in continuing of the project pass the initial simulation phase.The software design allowed the determination of the system characteristic parameters and the verification of the simulation and controller.

5.1 Software Requirements

5.1.1 Data Aquisition

Communication with the microcontroller was implemented using the serial communication from the external computer to the microcontroller. Communication with the microntroller occures differently depending on the state of the system. A *Python* script was used for communication that runs on the external computer.

If experiments are conducted the communication is uni-directional from the microcontroller towards the external computer. The microcontroller streams the state variables of the system to the external computer in specific structure shown in Figure 5.1. The star attached to the variables indicate that they are not sent in the correct units. The reason behind the decision is to reduce the processing time of the microcontroller. Sending data types such as floats are computational hungry and thus these conversions are handled on the external computer.

0	1	2	3	4	5	6	7
$	time	,	θ^*	,	ϕ^*	,	τ^*

Figure 5.1: Data Structure for Streaming Data during Experiments

The structure used in Figure 5.1 is chosen as comma-seperated values (.csv) which makes it easy to write these data in a .csv file and read them later to analyse the data.

The other state in which communication occured was bi-directional used for debugging purposes. In this state the *Python* script allows the user to type commands adhering to the structure shown in Figure 5.2. Based on the command used, the microcontroller would echo the same command back if it completed the command instructed.

0	1	2	3	4	...	n-1	n
$	cmd	,	value	value		\r	\n

Figure 5.2: Data Structure for Sending Commands

5.1.2 Embedded Program

Figure ?? shows the main execution flow of the microcontroller based on factors that influence their states. A brief overview of the execution flow is describe below.

On startup of the microcontroller, it will initialise the various peripherals required for operation. They include timers for PWM generation, ADC and interrupts for encoder signals. The microcontroller will than initialise the various variables required for operation.

Once initialisation is completed the microcontroller will check via an interrupt if a byte over the serial communication has been received. If a byte has been received it, the microncontroller will verify the command structure and execute based on this command.

Every 0.1ms the microcontroller will inspect the data arrays of the sampled signals. Direct Memory Access (DMA) is used for sampling and results in these sampling data being automatically refreshed by hardware.

The micrcontroller will than react whether a interrupt has occur to indicate a rising or falling edge of the encoder signal. This falling and rising edge indicates a incremental change of the position of the actuated pendulum the microcontroller will behave accordingly.

The microcontroller will than verify whether it is required to stream the data every 1ms to the external computer.

Chapter 6

Practical Results

6.1 Swingup Controller

6.2 Balancing Controller

6.3 Swingup and Balancing

Chapter 7

Conclusion

7.1 Summary

7.2 Recommendation

Add to the non-linear controller a integrated term controller that is beter with coulomb damping

Appendices

Appendix A

A.1 Derivation of the Mathematical Model

$$x_1 = l_1 \cos(\theta)$$
$$y_1 = -l_1 \sin(\theta)$$

$$x_2 = L_1 \sin(\theta) + l_2 \sin(\theta + \phi)$$
$$y_2 = -L_1 \cos(\theta) - l_2 \cos(\theta + \phi)$$

$$\dot{x_2} = L_1 \cos(\theta)\dot{\theta} - l_2 \cos(\theta + \phi)(\dot{\theta} + \dot{\phi})$$
$$\dot{y_2} = L_1 \sin(\theta)\dot{\theta} + l_2 \sin(\theta + \phi)(\dot{\theta} + \dot{\phi})$$

$$x_2^2 = L_1^2 \cos(\theta)^2\theta^2 + l_2^2 \cos(\theta + \phi)^2(\dot{\theta} + \dot{\phi})^2 + 2L_1 l_2 \dot{\theta}(\dot{\theta} + \dot{\theta}) \cos(\theta) \cos(\theta + \phi)$$
$$y_2^2 = L_1^2 \sin(\theta)^2\theta^2 + l_2^2 \sin(\theta + \phi)^2(\dot{\theta} + \dot{\phi})^2 + 2L_1 l_2 \dot{\theta}(\dot{\theta} + \dot{\theta}) \sin(\theta) \sin(\theta + \phi)$$

$$x_2^2 + y_2^2 = L_1^2\theta^2[\cos(\theta)^2 + \sin(\theta)^2] + l_2^2(\dot{\theta} + \dot{\phi})^2[\cos(\theta + \phi)^2 + \sin(\theta + \phi)^2] +$$
$$2L_1 l_2 \dot{\theta}(\dot{\theta} + \dot{\phi})[\cos(\theta) \cos(\theta + \phi) + \sin(\theta) \sin(\theta + \phi)]$$

Using the following trigonometric identities

$$\cos(\gamma)^2 + \sin(\gamma)^2 = 1$$

$$\cos(\gamma) \cos(\alpha) + \sin(\gamma) \sin(\alpha) = \cos(\gamma - \alpha)$$

the above equation resolves to:

$$V_2^2 = L_1\dot{\theta}^2 + l_2^2(\dot{\theta} + \dot{\phi})^2 + 2L_1 l_2(\dot{\theta} + \dot{\phi})\dot{\theta} \cos(\phi)$$

The kinetic energy in the system consist of the fixed rotation of the under-actuated pendulum and the rotation and velocity of the actuated pendulum.

$$T = \frac{1}{2}I_A\dot{\theta}^2 + \frac{1}{2}I_B(\dot{\theta}+\dot{\phi})^2 + \frac{1}{2}m_2V_2^2$$

$$T = \frac{1}{2}I_A\dot{\theta}^2 + \frac{1}{2}I_B(\dot{\theta}+\dot{\phi})^2 + \frac{1}{2}m_2[L_1\dot{\theta}^2 + l_2^2(\dot{\theta}+\dot{\phi})^2 + 2L_1l_2(\dot{\theta}+\dot{\phi})\dot{\theta}\cos(\phi)]^2$$

The potential energy in the system is defined as

$$V = -m_1gl_1\cos(\theta) - m_2g[L_1\cos(\theta) + l_2\cos(\theta+\phi)]$$

The Lagrange is defined as

$$\mathcal{L} = T - V$$

$$\mathcal{L} = \frac{1}{2}I_A\dot{\theta}^2+\frac{1}{2}I_B(\dot{\theta}+\dot{\phi})^2+\frac{1}{2}m_2[L_1\dot{\theta}^2+l_2^2(\dot{\theta}+\dot{\phi})^2+2L_1l_2(\dot{\theta}+\dot{\phi})\dot{\theta}\cos(\phi)]^2+m_1gl_1\cos(\theta)+ m_2g[L_1\cos(\theta)+l_2\cos(\theta+\phi)]$$

$$\frac{\partial\mathcal{L}}{\partial\theta} = -m_1gl_1\sin(\theta) - m_2gL_2\sin(\theta) - m_2gl_2\sin(\theta+\phi)$$

$$\frac{d}{dt}\frac{\partial\mathcal{L}}{\partial\dot{\theta}} = I_A\ddot{\theta}+I_B\ddot{\theta}+I_B\ddot{\phi}+m_2L_1^2\ddot{\theta}+m_2l_2^2\ddot{\theta}+m_2l_2\ddot{\phi}+2m_2L_1l2\ddot{\theta}\cos(\phi)-2m_2L_1l_2\dot{\theta}\dot{\phi}\sin(\phi)+ m_2L_1l_2\ddot{\phi}\cos(\phi) - m_2L_1l_2\dot{\phi}^2\sin(\phi)$$

$$\frac{\partial\mathcal{L}}{\partial\phi} = -m_2L_1l_2(\dot{\theta}+\dot{\phi})\dot{\theta}\sin(\phi) - m_2gl_2\sin(\theta+\phi)$$

$$\frac{d}{dt}\frac{\partial\mathcal{L}}{\partial\dot{\phi}} = I_B\ddot{\theta} + I_B\ddot{\phi} + m_2l_2^2\ddot{\theta} + m_2l_2^2\ddot{\phi} + m_2L_1l_2\ddot{\theta}\cos(\phi) - m_2L_1l_2\dot{\theta}\dot{\phi}\sin(\phi)$$

The differential equation describing the dynamics of the system is

$$\frac{d}{dt}\frac{\partial\mathcal{L}}{\partial\vec{\dot{q}}} - \frac{\partial\mathcal{L}}{\partial q} = B(\dot{q}) + \tau(q)$$

where $q = \begin{bmatrix}\theta\\ \phi\end{bmatrix}$

A.2 Collocated Linearisation

$$d_{11}\ddot{\theta} + d_{12}\ddot{\phi} + h_1 + \psi_1 = 0 \tag{A.1}$$

$$d_{21}\ddot{\theta} + d_{22}\ddot{\phi} + h_2 + \psi_2 = \tau \tag{A.2}$$

Starting from the condense equation (A.1) and (A.3), $\ddot{q_1}$ is solved in equation (A.1) and substituted in (A.1) resulting in

$$\bar{d_2}\ddot{\theta} + \bar{h_2} + \bar{\psi_2} = \tau \tag{A.3}$$

where the newly defined terms are given as:

$$\bar{d_2} = d_{22} - \frac{d_{21}d_{12}}{d_{11}}$$

$$\bar{h_2} = h_2 - \frac{d_{21}h_1}{d_{11}}$$

$$\bar{\psi_2} = \psi_2 - \frac{d_{21}\psi_1}{d_{11}}$$

τ can now chosen to linearise the terms in equation (A.3) as:
$\tau = \bar{d_2}v_2 + \bar{h_2} + \bar{\psi}$

A.3 Taylor Series Expansion Around Unstable Equilibrium Position

A.4 Communication Structure

0	1	2	3	4	...	n-1	n
$	cmd	,	value	value		\r	\n

Figure A.1: Data Structure for Sending Commands

In Table A.1 the various commmands that are used in the command structure shown in Figure A.1 used for debugging purposes is explained with the possible value ranges that can be used.

A.5 Electronic Design Schematic

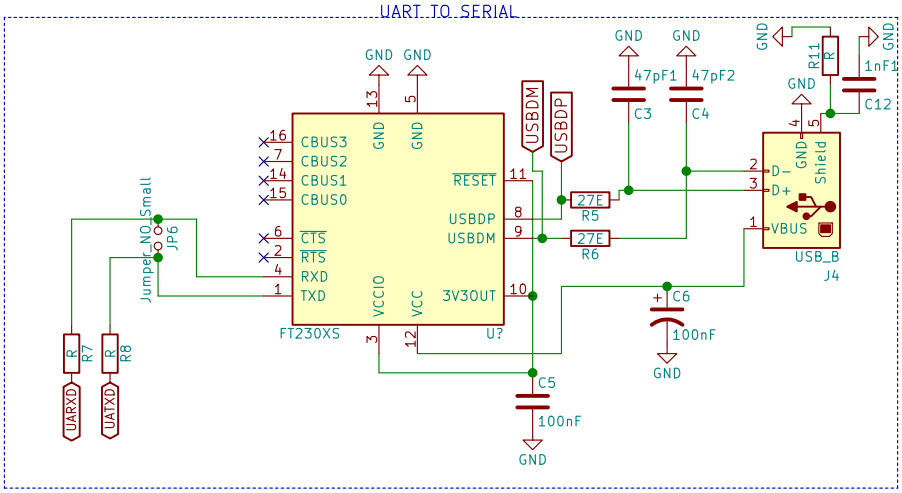

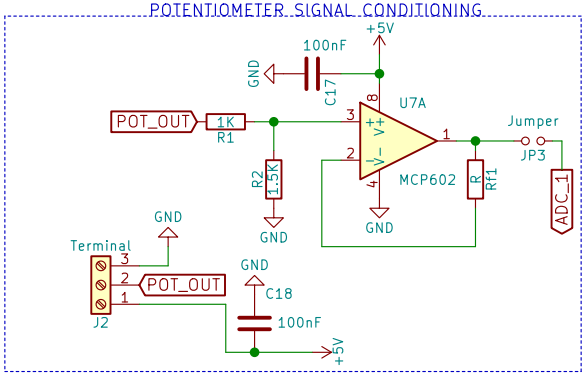

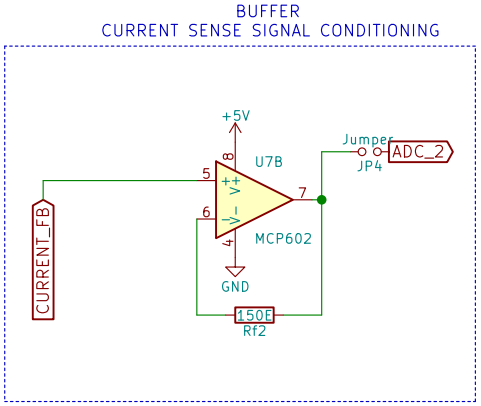

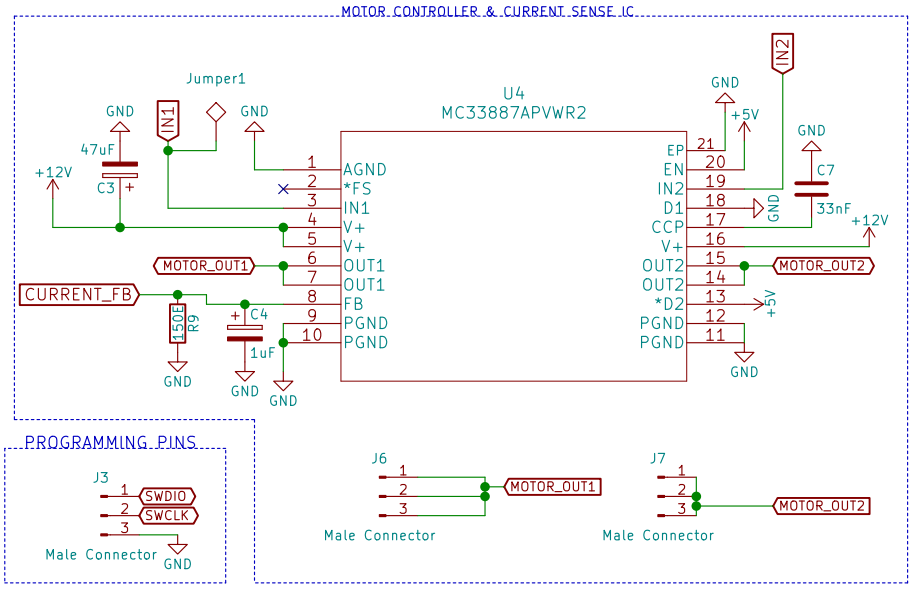

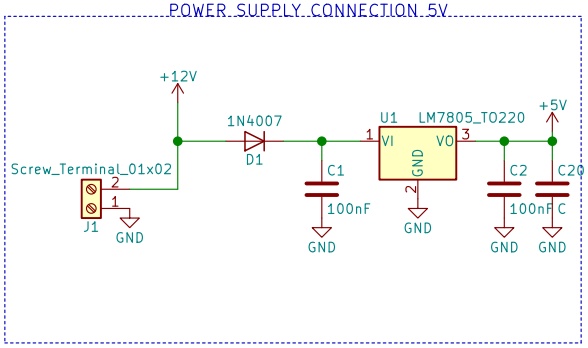

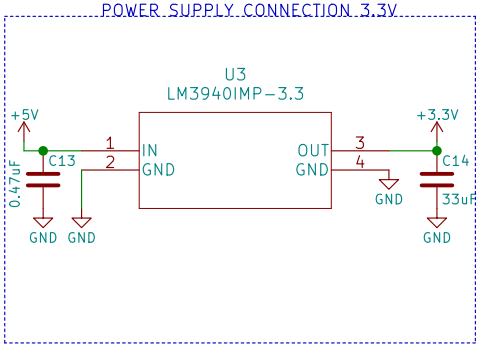

Sheet: /	
File: Acrobat.sch	
Title: Acrobat Schematic	
Size: A4	Date:
KiCad E.D.A. eeschema 4.0.7	Rev: Id: 1/3

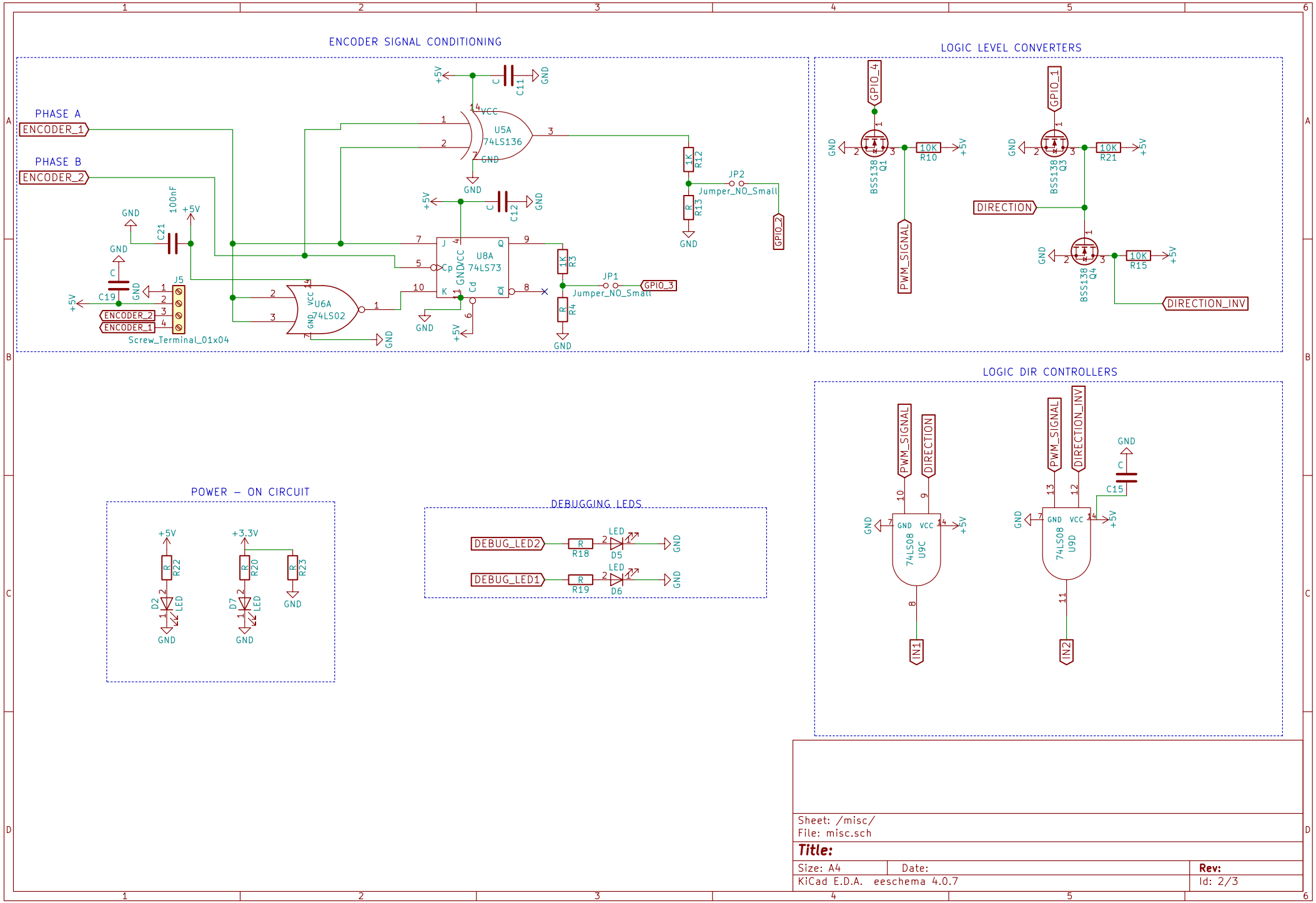
ENCODER SIGNAL CONDITIONING
PHASE A
ENCODER_1
PHASE B
ENCODER_2
U5A
74LS136
U6A
74LS02
U8A
74LS73
Screw_Terminal_01x04
Jumper_NO_Small
Jumper_NO_Small
GPIO_3
GPIO_2
LOGIC LEVEL CONVERTERS
GPIO_4
GPIO_1
BSS138
BSS138
BSS138
DIRECTION
PWM_SIGNAL
DIRECTION_INV
LOGIC DIR CONTROLLERS
74LS08
74LS08
IN1
IN2
POWER – ON CIRCUIT
DEBUGGING LEDS
DEBUG_LED2
DEBUG_LED1
LED
LED
Sheet: /misc/
File: misc.sch
Title:
Size: A4
Date:
Rev:
KiCad E.D.A. eeschema 4.0.7
Id: 2/3

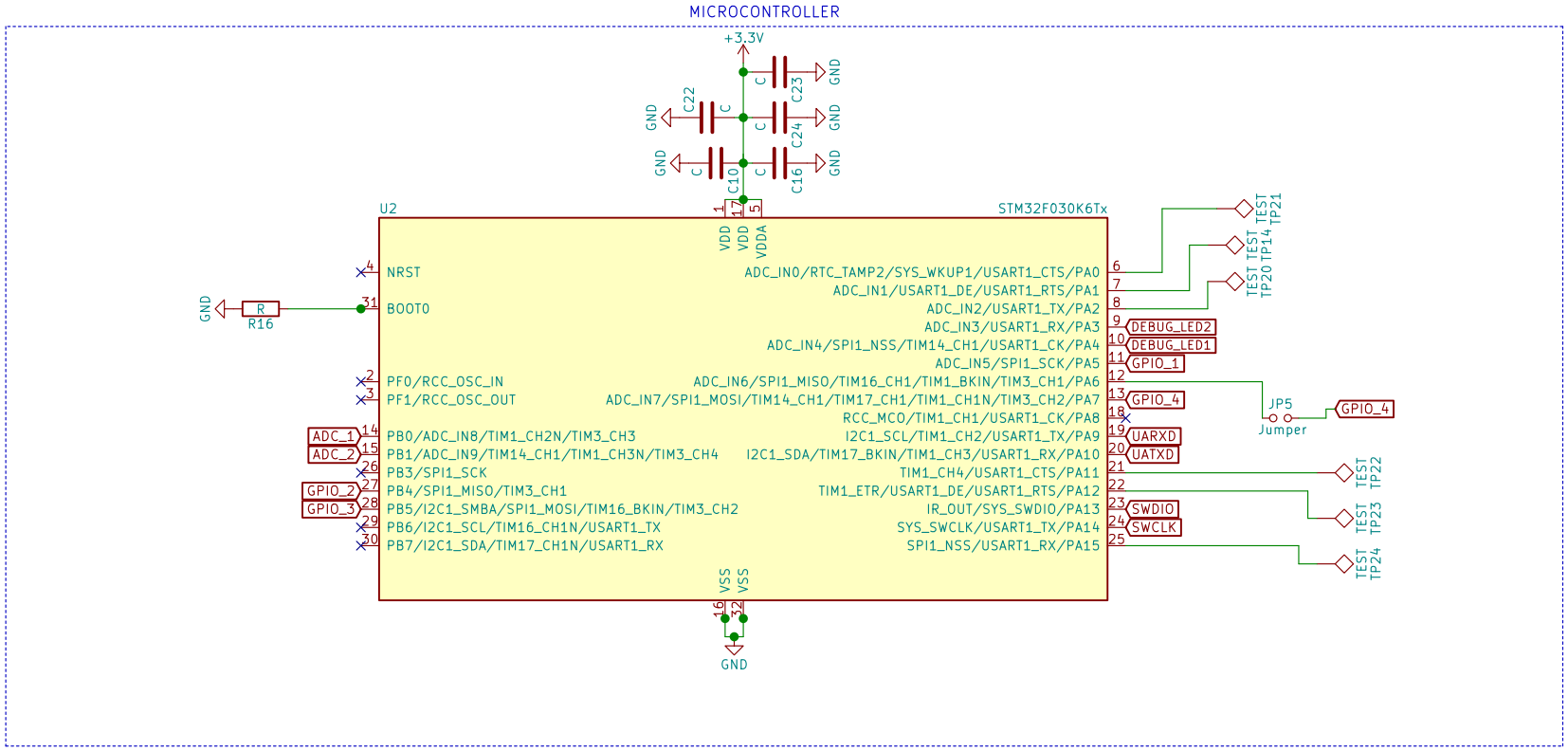

Sheet: /microcontroller/		
File: microcontroller.sch		
Title:		
Size: A4	Date:	**Rev:**
KiCad E.D.A. eeschema 4.0.7		Id: 3/3

Command	Range	Effect
A		
B		3.3
C		12

Table A.1: Summary of Communication Commands and their Effects

List of References

(1990). A case study in approximate linearization: The acrobat example. *Proc. American Control Conference*.

(1995). The swing up control problem for the acrobat. *IEEE Control Systems*, vol. 47, no. 10, pp. 50–55.

(2002). An explicit description of null controllable regions of linear systems with saturating actuators. *Systems & Control Letters*, vol. 47, no. 10, pp. 65–78.

(2007 2). *5.0 A H-Bridge woth Load Current Feeback*. Freescale Semiconductor, 12th edn. Document Number: MC33887.

(2017). *How to get the best ADC accuracy in the STM32 microcontrollers*. ST Electronics.

Faulhaber (2011). *Encoders, Magnetic Encoder, Series IE2-16*. Faulhaber, 11th edn.

Gene F. Franklin, J. David Powell, e.a. (2015). *Feedback Control of Dynamic Systems*. 7th edn. Pearson Education Limited, Edingburgh Gate, Harlow, Essex CM20 2JE, England. ISBN 1-29-206890-6.

Inman, D.J. (2015). *Engineering Vibration*. Pearson Education Limited.

Instruments, N. (2006 9). *Magnetic Encoder Fundamentals*. 10. National Instruments, The address.

Tedrake, R. (). Underactuated robotics: Algorithms for walking, running, swimming, flying, and manipulation (course notes for mit 6.832).
Available at: `http://underactuated.mit.edu/`